8-16-2019 10:00 AM

Monocyte MRI Relaxation Rates are Regulated by Extracellular Iron and Hepcidin

Praveen S.B Dassanayake
The University of Western Ontario

Supervisor
Goldhawk, Donna
Lawson Health Research Institute

Graduate Program in Medical Biophysics
A thesis submitted in partial fulfillment of the requirements for the degree in Master of Science

Abstract

Monocytes are an important immune cell type in chronic inflammatory conditions like atherosclerosis and heart failure. The increase in number of monocytes released to the peripheral blood circulation, the differentiation of monocytes to macrophages, and the presence of different macrophage subpopulations during pro- and anti-inflammatory stages of tissue injury may provide markers for monitoring inflammation. In particular, changes in monocyte iron metabolism during an inflammatory response may increase the possibility of tracking these immune cells non-invasively using magnetic resonance imaging (MRI). When secretion of the polypeptide hormone hepcidin is stimulated during inflammation, it binds the iron export protein ferroportin (FPN) on a limited number of cell types, including monocytes and macrophages. This ligand-receptor interaction leads to FPN internalization and downregulation through ubiquitin-mediated degradation. We hypothesized that hepcidin-mediated changes in monocyte iron regulation influence both cellular iron content and magnetic resonance (MR) relaxation rates. In response to varying conditions of extracellular iron supplementation, we observed THP-1 expression of FPN protein and its downregulation following hepcidin treatment. Also, in the presence hepcidin and iron supplementation, we detected a significant increase in the total transverse relaxation rate, R_2*, compared to non-supplemented cells. The positive correlation between total cellular iron content and R_2* improved from moderate to strong in the presence of hepcidin. These *in vitro* findings suggest that hepcidin-mediated changes detected in monocytes using MRI could be valuable for cell tracking *in vivo* during an inflammatory response.

Keywords

Magnetic resonance imaging, Monocytes, Iron export, Ferroportin, Hepcidin, Inflammation.

Summary (Lay abstract)

Background: Inflammation is important in many diseases like cancer, heart failure and atherosclerosis. Inflammatory responses have many roles, including tissue repair and the elimination of harmful pathogens. This is partly accomplished by limiting the amount of iron required for bacterial growth. Although inflammation is part of wound healing even in conditions like heart disease, excess inflammation can lead to changes in the size, shape and function of the heart and eventually to heart failure. Therefore, clinical management of inflammation by distinguishing between pro- and anti-inflammatory responses is important but remains challenging for many reasons. To understand when interventions should be introduced to prevent excess inflammation, we propose the use of Magnetic Resonance Imaging (MRI) to noninvasively detect the activity of immune cells (like monocytes, a type of white blood cell) that play a major role in inflammation. In our molecular imaging approach, we track changes in cellular iron metabolism using MRI since changes in iron are regulated by the hormone, hepcidin and reflect stage of inflammation.

Hypothesis: Hepcidin increases cellular iron content and MRI contrast in a laboratory model of human monocytes.

Methods: Monocytes are cultured for one week in the absence and presence of iron supplement and hepcidin, to mimic the cellular environment after a heart attack. Small volumes of these cultured cells are then placed in a clinical MRI scanner and imaged.

Results and Significance: When monocytes were exposed to hepcidin, we observed an increase in both cellular iron and MRI contrast. This research may improve how we monitor cells responding to inflammation signals like hepcidin, in patients with conditions like cancer, heart failure and atherosclerosis.

Acknowledgement

I would like to first thank my supervisor Dr. Donna Goldhawk for her support during my master's degree. You have been an excellent mentor and thank you for teaching me the basics in cell biology and cell culture. I am also thankful for our monthly meetings and guidance towards finishing my project.

Next, I would like to thank my advisory committee members Drs. Sean Gill and Blaine Chronik for their valuable feedback on my research. Also, I am thankful to our collaborators Drs. Frank Prato and Terry Thompson for their feedback throughout my study.

I would also like to thank the Goldhawk lab members for sharing their experience with me and giving me constructive feedback on my work. I would especially like to thank Khalid Abdalla, Sarah Donnelly, Daisy Sun, and Tian Tian Hou. Also, I would like to thank previous undergraduate students in our lab Olivia Sehl and Shalini Perugu for their contribution in wester blots. One of the immunoblotting images (Figure7A) I cultured the THP-1 cells as mentioned in the methods (Figure 5) at the end of the incubation time Olivia Sehl contributed for gel electrophoresis and blotting. Therefore, I would like to acknowledge her participation for Figure 7A. Additionally, I would like to thank John Butler, Heather Biernaski and Lynn Keenliside for the technical support during my research.

Importantly, I would like to thank my wife Nirmani Malge for encouraging me every step of the way and for her patience and kindness. Also, I would like to thank my wife for the sacrifices she had to make to help me pursue my studies. I am also grateful for my parents for their guidance and for supporting me both mentally and financially throughout my study. Special thanks go to my father who I always look up to and want to emulate in the future. I appreciate his valuable advice to me during my studies. In addition, I want to thank my two younger brothers for encouraging and supporting me. Thank you everyone for your support during my research project.

Table of content

List of figures

List of appendices

Chapter 1: Introduction

1.1 Systemic inflammatory response

Inflammation is induced in response to host cell defense mechanisms against pathogens or endogenous stress signals. Inflammation is also a driving factor in many diseases like atherosclerosis, cancer and heart failure. In these diseases, an inflammatory response facilitates the elimination of invading pathogens, clearance of necrotic cells and repair of damaged tissues. This entails recruitment of inflammatory cells like lymphocytes, monocytes and neutrophils to the inflamed site [1]. Among these cell types, monocytes are the most abundant immune cell and play a major role in chronic inflammatory conditions like atherosclerosis and heart failure [2]. There are three distinct monocyte subsets reported in the literature, which express select proteins to varying degrees as denoted by +/- nomenclature. These are a) classical, classification determinant (CD)$14^{++}CD16^{-}$ monocytes, b) intermediate $CD14^{++}CD16^{+}$ monocytes, and c) non-classical $CD14^{+}CD16^{++}$ monocytes. In conditions like acute myocardial infarction (AMI) — where blockage of the coronary artery by atherosclerotic plaque causes tissue hypoxia, destabilizing the cell membrane of cardiomyocytes and leading to cell death [3] — there is an increase in intermediate $CD14^{++}CD16^{+}$ monocytes [4, 5]. These intermediate monocytes, therefore, may become a potential target population for therapeutic applications related to tracking the inflammatory response in disease.

In response to growth factors and cytokines that are secreted during inflammation, infiltrating monocytes differentiate into macrophages [6]. Monocytes and macrophages produce a variety of cytokines, chemokines, growth factors and proteases to assist during both pro- and anti-inflammatory stages [7]. Pro-inflammatory cytokines and chemokines promote immune cell infiltration and host cell secretion of antimicrobial molecules to eliminate microorganisms and reduce the chance of infection [8]; whereas, anti-inflammatory cytokines and chemokines contribute to tissue repair and remodeling through phagocytosis of cell debris and inflammation resolution [9]. However, inflammation is not always successfully resolved, leading to inflammation associated disorders. For instance, chronic pro-inflammatory signaling may lead to hypoferremia

and tissue damage [10]. In conditions like AMI, a prolonged anti-inflammatory response can lead to left ventricular remodeling and heart failure [9].

Methods that differentiate between pro- and anti-inflammatory responses are needed to improve therapeutic interventions. For example, if anti-inflammatory therapy is administered too early, this may increase the risk of infection [1, 9]. Since monocytes are the most abundant immune cell type present in chronic inflammatory conditions, tracking these cells with magnetic resonance imaging (MRI) may be useful for noninvasively monitoring systemic inflammatory responses and enhancing treatment options.

1.2 Advancements in molecular imaging of inflammation

Imaging modalities, including magnetic resonance imaging (MRI), hyperpolarized MRI, positron emission tomography (PET) and single photon emission computed tomography (SPECT), can be used to monitor inflammation [11, 12]. These modalities are currently used to monitor severe myocardial fibrosis or scar tissue formation, which changes the shape and function of the left ventricle and contributes to heart failure [11, 13].

Ultrasound and X-ray computed tomography (CT) have also proven useful in imaging inflammation in conditions like heart failure [14]. Nuclear medicine imaging using PET and SPECT have been applied to detect changes in molecular signaling pathways during inflammation [11]. Radioactive tracers used in PET and SPECT can be developed that bind to specific receptors on inflammatory cells, enabling cell tracking during an inflammatory response [15]. PET and SPECT scanners are commonly integrated with CT or MRI. Hybrid PET-CT and PET-MRI scanners allow for localization of molecular signaling during inflammation with high-resolution anatomical images [11, 16].

Several clinically relevant PET tracers can be used to monitor inflammation. ^{18}F-fluorodeoxyglucose (FDG) PET can be used to assess myocardial viability post-AMI through differences in glucose utilization by cardiac tissue. This can be used to monitor recovery of the damaged myocardium as tracer uptake improves with revascularization, tissue healing and regeneration. FDG has also been used to monitor arterial inflammation in atherosclerosis, implicating macrophages in atherosclerotic plaques [17, 18]. Pentixafor, a ^{68}Ga labelled PET tracer for monitoring inflammation, binds the C-X-C

chemokine receptor type 4 (CXCR4) that promotes leukocyte extravasation during inflammation [19]. Studies have shown increased uptake of Pentixafor in the initial stages of AMI [19, 20]. Isoquinoline carboxamide is a ^{11}C labelled PET tracer used to monitor neuroinflammation in diseases like dementia [21]. This PET tracer acts as a ligand for translocator protein (TSPO) a transmembrane domain protein expressed in the outer mitochondrial membrane of microglia which is substantially upregulated in response to neuroinflammation [21]. Among the PET tracers above, ^{18}F-FDG is most commonly used for imaging inflammation. However, ^{18}F-FDG is taken up by monocytes, macrophages and other glucose metabolizing cells (muscle, brain, etc.) involved in pro- and anti-inflammatory responses at the site of inflammation, causing difficulties in differentiating between these two stages of the inflammatory response. PET also uses ionizing radiation which may limit its application in certain populations, including children and pregnant women. Although PET has superior sensitivity, its spatial resolution is inferior to other imaging modalities like MRI.

MRI is a non-invasive imaging modality with high spatial resolution [22]. MRI can be used to study cardiac function, anatomy, inflammation post-AMI and myocardial stiffness. MRI is also used to monitor inflammation in conditions like breast cancer [22, 23]. The use of contrast agents in MRI significantly improves the detection of inflamed tissue [24]. Gadolinium chelates are useful as exogenous contrast agents in monitoring inflammatory responses [25, 26]. Magnetic iron oxide nanoparticles (MNPs) are advantageous in monitoring scarce molecular targets related to inflammation, as these are small biologically inert molecules with high magnetic relaxation properties [26]. During an inflammatory response, MNPs are considered foreign bodies by innate immune cells and will be phagocytosed, enabling enhanced visualization of these inflammatory cells [26]. Perfluorocarbon nano-emulsions (^{19}F) are also considered useful probes for imaging inflammation. Like MNPs, these ^{19}F nano-emulsions are taken up by phagocytes during their migration to the site of inflammation, enabling detection of these cells in response to inflammation [24]. Overall, use of nonionizing radiation for repetitive imaging, high image resolution, multi-parametric imaging and hybrid imaging are the advantages of using MRI over other imaging modalities to monitor inflammation [27].

1.3 Systemic and cellular iron regulation

1.3.1 Cellular iron regulation

Iron is an important element for all living cells, required for DNA synthesis, respiration and oxygen transport [28]. However, excessive iron is cytotoxic and can cause diseases like cirrhosis and cardiomyopathy. Increased iron in regions of the brain has been linked to neurodegenerative diseases like Parkinson's and Alzheimer's [29]. On the other hand, iron deficiency can also be deleterious, causing cognitive defects in children as well as anemia in adults. Therefore, cellular iron content must be maintained within a narrow range through iron homeostasis to avoid adverse effects.

Under normal conditions, 1–2 mg of dietary iron enters the serum daily via enterocytes of the small intestine [30]. Cellular iron regulation is mediated by several proteins which are regulated at transcriptional, post-transcriptional and post-translational levels. In mammals, serum iron is bound to a protein called transferrin (Tf, Figure 1). Each Tf molecule can bind two iron atoms in the ferric state (Fe^{+3}). Tf-bound iron is internalized by cells through a receptor-mediated process involving transferrin receptor (TfRc) [30, 31].

Following cellular iron uptake, the reducing environment of the vesicle causes a transition from Fe^{+3} to the ferrous state (Fe^{+2}). Fe^{+2} is then transported by a transmembrane protein found on the vesicle that was endocytosed, the divalent metal transporter (DMT 1), into the labile iron pool (LIP, Figure 1), a transitory redox active source of iron. Some of the iron in the LIP is then shuttled to ferritin protein complexes where it is oxidized and stored as Fe^{+3} [32]. There are two main ferritin subunits which are heavy (H) and light (L) ferritin. H-ferritin functions as a ferroxidase and facilitates oxidation of Fe^{+2}. While some of the imported iron is used by intracellular processes, certain cells like monocytes and macrophages also export iron through ferroportin (FPN, Figure 1) [30, 33, 34].

The iron response proteins (IRPs), IRP1 and IRP2, regulate iron uptake, storage, and export. When intracellular iron content is low, IRPs bind to iron response elements (IREs) on the 5' end of the mRNA for ferritin and FPN to block translation and increase

cellular iron availability. In addition, under iron depleted conditions, IRPs bind to IREs on the 3ˈ end of TfRc mRNA to suppress its degradation, thereby increasing translation of TfRc [31, 35]. Conversely, in iron replete conditions, IRPs do not bind to IREs; causing more ferritin translation for extra iron storage, increasing translation of FPN for iron efflux and, lastly, downregulating TfRc mRNA to prevent more iron influx [30].

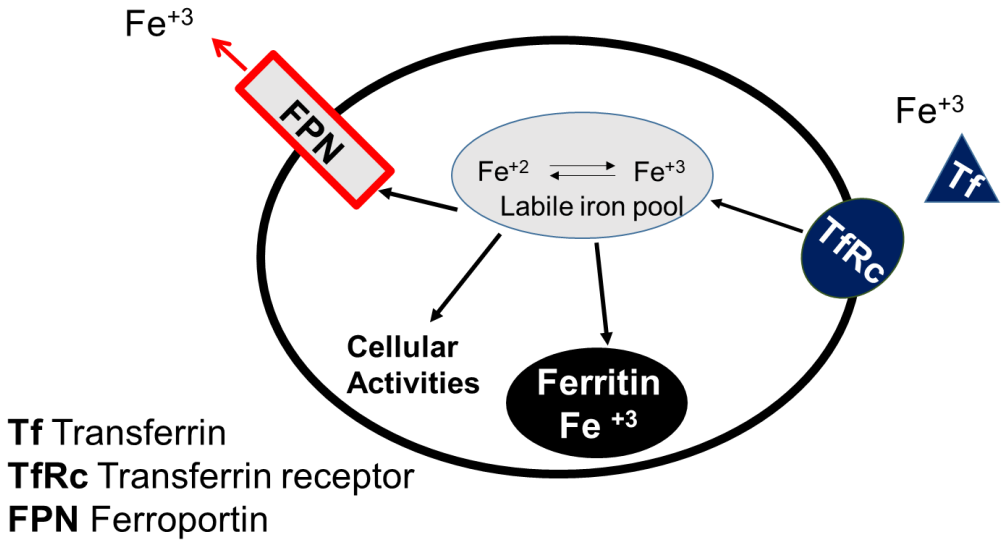

Figure 1. Key features of mammalian iron regulation. Serum iron is mainly bound to transferrin (Tf) and imported into cells through receptor-mediated endocytosis by the transferrin receptor (TfRc). While a small amount of iron in the labile iron pool (LIP) is available for cellular activities, most intracellular iron is stored in ferritin. Only select cells, including monocytes and macrophages, export iron through ferroportin (FPN). The endocrine hormone, hepcidin, secreted from liver hepatocytes in response to inflammation and high serum iron, downregulates FPN.

1.3.2 Systemic iron homeostasis in humans

Iron is essential to survival at the cellular level, but it plays an equally important role systemically. Dietary iron enters the circulation *via* enterocytes in the duodenum [36]. This is a crucial process, enabling hematopoiesis in the bone marrow (Figure 2). Although some iron is used for the generation of leukocytes and innate immune cells, most of the iron goes towards erythropoiesis. Approximately 22 mg of transferrin-bound iron per day is used to generate erythrocytes in the bone marrow and to produce hemoglobin. In fact, approximately 60-70% of the body's iron resides in red blood cells [36].

Old and damaged red blood cells are recycled within the spleen and this essential process maintains the necessary iron levels, even when dietary iron uptake is limited. Macrophages and monocytes, the phagocytic cells in the reticuloendothelial system, recycle red blood cells to release iron trapped in hemoglobin. Recycled iron is then released into the circulation to be reused. Since erythropoiesis uses so many resources each day, the mechanisms responsible for recycling iron satisfy this daily requirement [36, 37].

As at the cellular level, excess systemic iron can be dangerous; therefore, close to 20% of total iron is sequestered and stored within splenic macrophages and hepatocytes [36]. Systemic iron homeostasis is a tightly regulated process; for example, iron demand increases following blood loss, promoting the release of iron from macrophages, hepatocytes, and enterocytes. Once the demand for iron is alleviated, iron export from FPN-expressing cells decreases to maintain iron homeostasis [36, 38].

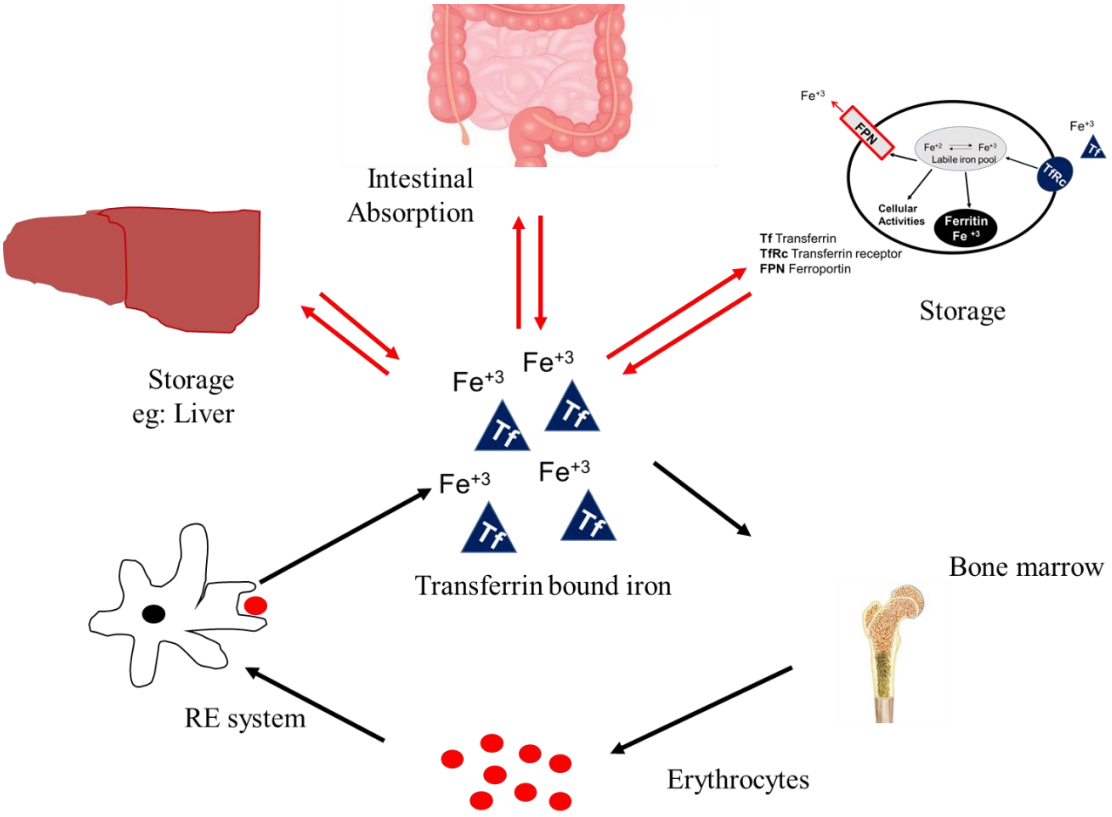

Figure 2. Systemic iron regulation. Dietary iron is secreted into the circulation by enterocytes within the proximal small intestine. Circulating iron is then bound by proteins like transferrin. Transferrin-bound iron is transported through the circulation where it is used for hematopoiesis (mainly erythropoiesis) in the bone marrow. Damaged and old erythrocytes are removed from the bloodstream by macrophages in the reticuloendothelial (RE) system within the spleen and the iron is recycled back to the plasma. While all cells maintain stores of iron, hepatocytes, monocytes and macrophages store sizable amounts of iron [36].

1.3.3 Controlled regulation of iron export protein (FPN)

The iron export protein FPN plays a vital role in regulating both systemic and cellular iron homeostasis. Both processes are tightly controlled to ensure survival and prevent disease. This includes regulation of FPN at transcriptional, post-transcriptional and post-translational levels [39] all of which permit fine-tuned control of iron homeostasis.

Btb and Cnc homology 1 (Bach1), a basic leucine zipper transcriptional repressor, controls FPN expression at the transcriptional level. When the antioxidant response element (ARE) in the promoter of *FPN* is bound by Bach1, *FPN* transcription is repressed, limiting FPN mRNA production and overall FPN protein levels. Heme reverses this process by causing the degradation of Bach1 and promoting ARE binding to nuclear factor erythroid 2-like (NRF2) protein, leading to transcriptional activation of *FPN* [40].

Iron also affects FPN expression in monocytes and macrophages at the post-transcriptional level. FPN mRNA has a 5´ IRE, which binds to IRPs under iron deficient conditions, repressing FPN expression [41].

At the post-translational level, FPN is controlled hormonally. When the polypeptide hormone hepcidin binds to FPN, it causes FPN internalization and degradation [42]. Hepcidin is released by hepatocytes during iron overload to prevent iron export from cells and limit plasma iron levels. Together, these different forms of FPN regulation allow for effective and reliable control of systemic and cellular iron metabolism under various circumstances.

1.4 Effect of hepcidin on monocyte iron regulation

Healthy humans maintain a plasma iron concentration between 5–30 μM and store approximately 0.2–1.0 g of iron within the cellular compartment. To maintain these healthy levels, iron absorption is increased in iron deficiency and decreased in iron overload conditions. These observations led to the discovery of hormonal iron regulation in mammals. The 25 amino acid polypeptide hormone hepcidin, post-translationally regulates iron export. Hepcidin acts as a ligand for the cell surface, iron export protein FPN, causing its phosphorylation, internalization and degradation, as mentioned above [43]. Following hepcidin binding to FPN, it will be phosphorylated then ubiquitin ligases add ubiquitin tags onto FPN, promoting its endocytosis (Figure 3). The polyubiquitin tail signals FPN for degradation via the lysosome, a protein complex containing proteases [44, 45]. This process decreases iron export in FPN-expressing monocytes, macrophages, enterocytes and hepatocytes. Between 10–100 nM hepcidin is required for FPN downregulation [43]. Hepcidin expression is controlled by plasma iron levels, erythropoietic needs, as well as inflammation. In response to increased plasma iron, the bone morphogenetic protein (BMP) and mothers against decapentaplegic (SMAD) pathways upregulate hepcidin transcription in hepatocytes. When BMP6 binds to its receptor in the presence of the co-receptor hemojuvelin, the SMAD signaling cascade is activated. The end result of this signaling pathway is phosphorylated SMAD protein complexes, translocating to the nucleus, binding to the 5ˈuntranslated region of the *hepcidin* gene and enhancing its transcription, thereby increasing hepcidin levels [46, 47].

Hepcidin expression is upregulated during infection, acting as an anti-microbial peptide by decreasing the availability of circulating iron — an important cofactor for many pathogens [48]. In hepcidin deficient conditions like hereditary hemochromatosis, patients are more susceptible to certain bacterial infections caused by pathogens like *Listeria monocytogenes* due to excess iron in the plasma promoting bacterial growth [49].

Previous studies have shown increased expression of hepcidin mRNA in freshly isolated monocytes as well as in the human monocytic cell line THP-1 in response to proinflammatory mediators like lipopolysaccharide or interleukin (IL)-6 [50, 51]. However, the level of hepcidin mRNA expression in THP-1 cells was significantly lower

than that of liver hepatocytes. Monocytes express hepcidin for autocrine or paracrine regulation of FPN; however, the endocrine expression of hepcidin by hepatocytes far exceeds that of monocytes [52]. Since monocytes phagocytose damaged red blood cells, iron storage may increase in these cells during a pro-inflammatory response as increased levels of hepcidin downregulate FPN and prevent iron export [52, 53]. However, during an anti-inflammatory response, low hepcidin levels promote iron efflux from monocytes (through FPN), allowing more iron in plasma [42].

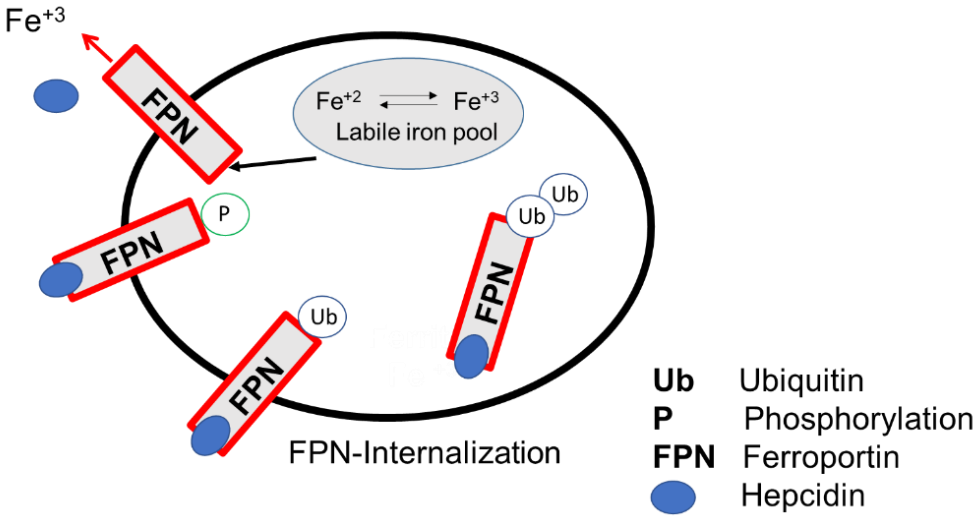

Figure 3. Hepcidin-mediated FPN degradation. Certain cells including monocytes and macrophages export iron through the protein ferroportin (FPN). When the hormone hepcidin is expressed, it acts as a ligand and binds FPN resulting in FPN phosphorylation. This is followed by ubiquitination by ubiquitin ligases. FPN ubiquitination drives its endocytosis where FPN is further ubiquitinated and degraded by the lysosome, thereby reducing iron export. In iron deficient conditions, hepcidin levels are reduced to enable FPN to export iron.

1.5 Magnetic resonance imaging (MRI)

To better understand how variations in cellular iron content affect the magnetic resonance (MR) relaxation rates, MR physics will be discussed below.

MRI is a noninvasive imaging modality with high spatial resolution and is used for the detection, diagnosis and monitoring of various medical treatments. The technology is based on the excitation of hydrogen atoms (protons) largely found in water molecules within tissues. This MR signal is then converted to an image, giving anatomical information about the subject [54].

Protons within the atomic nuclei of hydrogen atoms have magnetic properties represented as nuclear spins. Thus, protons behave as tiny magnets with a magnetic moment (μ) that precesses randomly. The vector sum of all these magnetic moments is called the net magnetization vector (M_0). Normally, the vector of these spinning magnetic moments is randomly distributed, leading to no net magnetization ($M_0 = 0$). In the presence of an external magnetic field (B_0), slightly more protons will align with B_0 (parallel) than against B_0 (anti-parallel), which creates a net magnetization in the direction of the B_0 field (z-direction) [53]. Nuclear spins precess about the axis of the applied external magnetic field (B_0) at the Larmor frequency (ω_0) in radians/second, which is proportional to B_0 in Tesla (T) as shown below. Larmor frequency (ω_0) increases linearly with B_0, and is also dependent on the gyromagnetic ratio (γ), a physical constant specific to the nuclei being imaged ($\gamma/2\pi = 42.58$ MHz/T for hydrogen protons) [54].

$$\omega_0 = \gamma B_0 \qquad (1)$$

The magnetic vector representing precessing protons can be broken down into two components: the longitudinal component (M_z) aligned with the direction of B_0 (z-direction) and the transverse component (M_{xy}) within the XY plane. Precession leads to rotation of the transverse component about the longitudinal (Z) axis. When spinning protons are subjected to B_0 there are more low energy state spins aligned parallel with B_0. The spins aligned against B_0 are considered to be in a high energy state. Since an excess of spins aligns with B_0, net/macroscopic magnetization has a longitudinal component

along the z-axis (M_z). Though the spins are rotating, but not in phase with each other, there is a null transverse microscopic magnetization ($M_{xy} = 0$) [54].

Exchanging energy between two systems at a specific frequency is known as resonance. In MR, energy is exchanged between nuclear spins and an applied radiofrequency (RF) field which is a small magnetic field represented by B_1. Only the protons that precess at the same frequency as the RF pulse (B_1) will exchange energy with that RF pulse. Once B_1 is applied, absorption of electromagnetic energy by the hydrogen nuclei will modify the spin equilibrium of the hydrogen protons. This is called excitation [54]. When these excited protons return to spin equilibrium, there is an emission of electromagnetic energy. Excitation of these protons causes changes to their energy levels and spin phases. At the quantum level, excitation leads to protons shifting from low energy state (parallel) to a high energy state (anti-parallel). This shift leads the macroscopic net magnetization vector to move to the XY plane. When considering the rotating frame of reference (Figure 4), net magnetization tips down during excitation and the flip angle (α°) is a function of the strength and duration of the RF pulse [54].

As described above, the net magnetization has two components, the longitudinal component (M_z) and transverse component (M_{xy}). During excitation, longitudinal magnetization (M_z) decreases and transverse magnetization (M_{xy}) appears except for a 180˚ flip angle (α°). As mentioned above, longitudinal magnetization is due to a different number of spins in parallel and anti-parallel states, and transverse magnetization is due to several spins getting into phase coherence. For example, during an excitation using an RF pulse with 90˚ flip angle, there is a null longitudinal magnetization ($M_z = 0$) due to an equal number of parallel and anti-parallel spins, but transverse magnetization (M_{xy}) exists due to all spins being in phase [54].

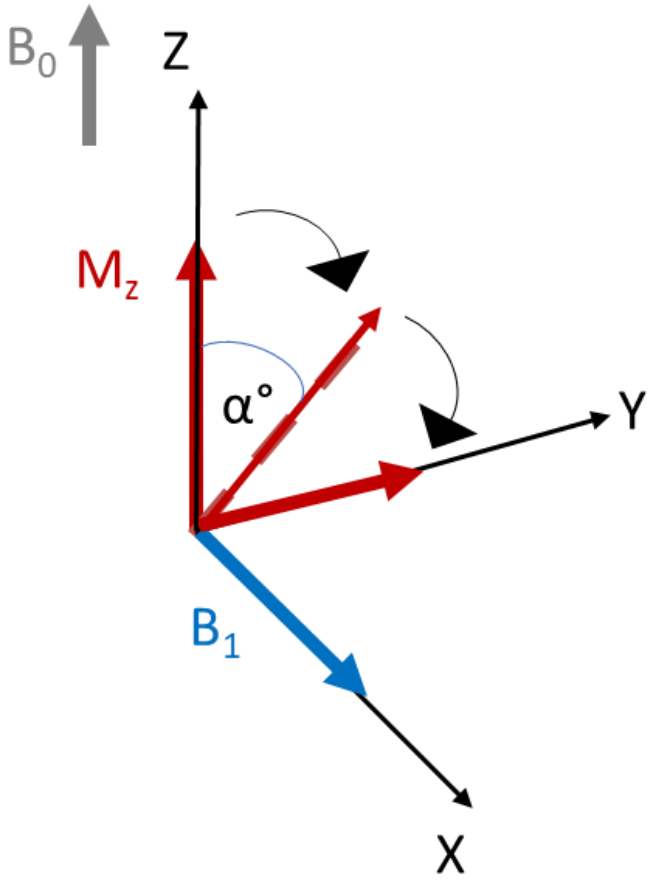

Figure 4. Rotating frame of reference. Longitudinal magnetization (M_z) in the presence of an RF field (B_1) tips down to the transverse plane (XY). Flip angle (α°) is a function of the strength and duration of B_1.

Return of the excited spins to the equilibrium value M_0 is called relaxation. During relaxation, the energy absorbed from B_1 is emitted as a nuclear magnetic resonance (NMR) pulse. Relaxation combines two different mechanisms; longitudinal relaxation refers to the recovery of longitudinal magnetization and transverse relaxation refers to the decay of transverse magnetization. During longitudinal relaxation, energy is exchanged between the spins and surrounding lattice (spin-lattice relaxation). As spins lose energy from the high energy state to a low energy state, absorbed RF energy is released to the surrounding lattice. An exponential curve can be fitted to the recovery of longitudinal magnetization. The time taken for longitudinal magnetization (M_z) to reach 63% of its original value is called the longitudinal relaxation time (T_1) as shown below [54].

$$\mathbf{M_z = M_0 \left(1 - \exp^{-(t/T1)} \right)} \qquad (2)$$

Transverse relaxation occurs due to dephasing of spins. When spins start to move together due to spin-spin interactions, their magnetic fields start to interact with each other. These spin-spin interactions, therefore, cause a cumulative loss in phase resulting in transverse magnetization decay. The decay of transverse magnetization (M_{xy}) is proportional to the acquired MR signal from the RF elements. The decrease in the signal intensity over time due to transverse relaxation is called free induction decay (FID). The decay of transverse magnetization can also be described by an exponential curve, where the time taken for transverse magnetization to decay up to 63% from its original value is the transverse relaxation time (T_2) as show below [54].

$$\mathbf{M_{xy} = M_0 \exp^{-(t/T2)}} \qquad (3)$$

Local magnetic field inhomogeneities may increase the decay of transverse magnetization (M_{xy}), resulting in an even shorter relaxation time, denoted by T_2*. Relaxation values are tissue specific and T_2 values are always shorter than T_1. The three relaxation time constants (T_1, T_2 and T_2*) can be interpreted as relaxation rates as follows: $R_1 = 1/T_1$, $R_2 = 1/T_2$ and $R_2^* = 1/T_2^*$. In order to determine the rate of decay of transverse relaxation related to local magnetic field inhomogeneities, denoted by R_2', the

difference between R_2* (due to spin-spin interactions and local magnetic field inhomogeneities) and R_2 (due to only spin-spin interactions) should be calculated [54].

$$R_2' = R_2^* - R_2 \qquad (4)$$

MRI has been evolving for many years, leading to improvements in the quality and speed of the signal acquisition. Each MRI sequence combines RF pulses and gradient magnetic fields to acquire a signal. Various MRI sequences have been established and depending on the type of sequence selected, the end goal is to acquire signals faster while minimizing image artifacts and maximizing the signal to noise ratio (SNR) [54].

There are three main components of a sequence: RF pulses which are essential for the excitation (and subsequent relaxation) of hydrogen protons; gradient pulses which are used for spatial encoding; and arrangement of the gradient pulse which is used to determine how the k space (defined as an array of numbers representing spatial frequencies in the MR image) is filled, using different echo types to read the signal (*e.g.* spin echo, gradient echo; described below) [54].

1.5.1 Spin echo sequence

Initially in the spin echo (SE) sequence, a 90˚ pulse is applied to tip the net magnetization in the Z axis into the XY plane. After the 90˚ pulse, a 180˚ pulse is applied at half of the echo time (TE/2). The purpose of the 180˚ pulse is to compensate for dephasing of the spins aligned in different positions in the XY plane, due to magnetic field inhomogeneities. Therefore, the 180˚pulse is used to re-phase the spins to obtain an echo that is weighted by T_2. In a SE sequence, echo time (TE) is defined as the time interval between the 90˚ pulse and the signal acquisition at echo. The repetition time (TR) is the time interval between two 90˚ RF pulses. At TR, the SE sequence will be repeated, with each repetition filling a line of k space [54].

1.5.2 Inversion recovery spin echo sequence

The inversion recovery SE sequence is used to obtain T_1 weighted images and it is similar to that of the spin echo sequence (section 1.5.1). However, a 180° RF pulse (inversion pulse) is applied prior to the 90° excitation pulse to invert the longitudinal magnetization M_z. The time between the inversion pulse and 90° excitation pulse is called the inversion time (TI) [54].

1.5.3 Gradient echo sequence

The gradient echo (GE) sequence uses a single RF pulse. The flip angle of the RF pulse applied in the GE sequence, denoting amount of spins tipped into the transverse plane, is always lower than 90˚. The consequence of using a lower flip angle for excitation is a faster recovery of the longitudinal magnetization, resulting in a decreased scan time. With the absence of a 180˚ pulse to re-phase spins, the loss of signal (T_2*) is proportional to spin-spin interactions (T_2) and magnetic field inhomogeneities [54].

1.5.4 Tissue contrast and effect of iron on magnetic resonance signal

Depending on TR,TE, and pulse sequence, different signal intensities between two tissues can be explained by their proton density, T_1 and T_2. For example, by setting TR to shorter values, relative intensities of two tissues are distinguishable by their T_1. This is called T_1-weighted imaging. However, by setting TR to longer values, the T_1 effect will be reduced and, given longer TE, tissue signal intensities will be altered by T_2. This is called T_2-weighted imaging. These changes in tissue contrast depending on TR and TE are further enhanced by the use of contrast agents. Contrast agents will shorten the T_1 and T_2 relaxation times of hydrogen nuclei located in their vicinity. Shortening of T_1 will brighten the MR images while shortening of T_2 will reduce the signal intensity and consequently darken the MR image [55]. Iron is a paramagnetic material which (in sufficient concentration) concentrates main magnetic field lines, creating field inhomogeneities resulting in faster dephasing of excited hydrogen protons in cells, thereby shortening T_2 [56, 57]. Depending on the iron handling ability of different cell

types, this effect may enhance future possibilities of tracking the cells based on fluctuations in the MR signal.

1.6 Overview of the thesis

Monocytes are the most abundant cell type responding to chronic inflammatory diseases like atherosclerosis [18]. Since the number of monocytes released to the peripheral circulation is increased during an inflammatory response [18, 58], tracking these monocytes could provide a diagnostic tool for monitoring chronic inflammatory conditions such as atherosclerosis and heart failure [18]. Moreover, different monocyte sub-populations reflect pro- and anti-inflammatory stages and may serve as markers of the inflammatory process in specific tissues, like the failing heart [5, 6].

The connection between inflammation and iron metabolism is specific to only a few cell types, including monocytes and macrophages, and raises the interesting possibility of tracking inflammation non-invasively using MRI. The polypeptide hormone hepcidin is secreted by the liver in response to inflammation. As the ligand for FPN, the iron export protein, hepcidin causes its post-translational degradation [59, 60]. This change in iron metabolism may influence MRI relaxation rates as M1 macrophages with relatively low FPN expression generally display an iron storage phenotype while M2 macrophages with generally high FPN expression typically exhibit iron recycling activity. Since monocytes are the precursors of macrophages, we investigated hepcidin-mediated changes in iron regulation and how it affects MR relaxation rates using the human THP-1 monocytic cell line.

1.7 Hypothesis

Hepcidin-mediated changes in monocyte iron regulation influence both cellular iron content and MR relaxation rates.

1.8 Objectives

The first objective was to investigate the expression of FPN in THP-1 monocytes. Changes in FPN expression in response to changes in extracellular iron were assessed by

Western blotting. We expected that THP-1 monocytes would express iron export protein in the presence of an extracellular iron supplement. Once the pattern of FPN expression was established, we investigated the effect of hepcidin on FPN degradation. Based on the literature, we expected FPN expression would be downregulated in response to hepcidin [44, 52, 61].

The second objective was to characterize MR relaxation rates in THP-1 monocytes in response to changes in extracellular iron supplementation. MRI experiments were conducted to obtain the baseline MR signal (-Fe), the iron-supplemented MR signal (+Fe) and the MR signal after iron supplement was withdrawn from culture for 1, 2, 4 and 24 hours. Results were compared to cells cultured in the presence of hepcidin. In response to hepcidin downregulation of FPN, we expected to see an increase in the MRI signal as intracellular iron levels increased.

The third objective was to determine the total cellular iron content of THP-1 monocytes and examine the correlation to MR relaxation rates, in the presence and absence of both iron supplement and hepcidin. Inductively-coupled plasma mass spectrometry (ICP-MS) was used to determine the total cellular iron content. We expected that elemental iron content would increase in the presence of hepcidin and iron supplementation.

References

1. Ong SB, Hernandez-Resendiz S, Crespo-Avilan GE, Mukhametshina RT, Kwek XY, Cabrera-Fuentes HA, Hausenloy DJ: **Inflammation following acute myocardial infarction: Multiple players, dynamic roles, and novel therapeutic opportunities**. *Pharmacol Ther* 2018, **186**:73-87.
2. Nunez J, Nunez E, Bodi V, Sanchis J, Minana G, Mainar L, Santas E, Merlos P, Rumiz E, Darmofal H: **Usefulness of the neutrophil to lymphocyte ratio in predicting long-term mortality in ST segment elevation myocardial infarction**. *Am J Cardiol* 2008, **101**(6):747-752.
3. Dewood MA, Spores J, Notske R, Mouser LT, Burroughs R, Golden MS, Lang HT: **Prevalence of total coronary-occlusion during the early hours of transmural myocardial-infarction**. *N Engl J Med* 1980, **303**(16):897-902.
4. Rogacev KS, Cremers B, Zawada AM, Seiler S, Binder N, Ege P, Grosse-Dunker G, Heisel I, Hornof F, Jeken J: **CD14++CD16+ Monocytes independently predict cardiovascular events**. *J Am Coll Cardiol* 2012, **60**(16):1512-1520.
5. Belge KU, Dayyani F, Horelt A, Siedlar M, Frankenberger M, Frankenberger B, Espevik T, Ziegler-Heitbrock L: **The proinflammatory CD14(+)CD16(+)DR(++) monocytes are a major source of TNF**. *J Immunol* 2002, **168**(7):3536-3542.
6. Wrigley BJ, Lip GYH, Shantsila E: **The role of monocytes and inflammation in the pathophysiology of heart failure**. *Eur J Heart Fail* 2011, **13**(11):1161-1171.
7. Ludwiczek S, Aigner E, Theurl I, Weiss G: **Cytokine-mediated regulation of iron transport in human monocytic cells**. *Blood* 2003, **101**(10):4148-4154.
8. Orn S, Breland UM, Mollnes TE, Manhenke C, Dickstein K, Aukrust P, Ueland T: **The chemokine network in relation to infarct size and left ventricular remodeling following acute myocardial infarction**. *Am J Cardiol* 2009, **104**(9):1179-1183.
9. Frangogiannis NG: **The inflammatory response in myocardial injury, repair, and remodelling**. *Nature Reviews Cardiology* 2014, **11**(5):255-265.

10. Nemeth E, Rivera S, Gabayan V, Keller C, Taudorf S, Pedersen BK, Ganz T: **IL-6 mediates hypoferremia of inflammation by inducing the synthesis of the iron regulatory hormone hepcidin**. *J Clin Invest* 2004, **113**(9):1271-1276.
11. Curley D, Plaza BL, Shah AM, Botnar RM: **Molecular imaging of cardiac remodelling after myocardial infarction**. *Basic Res Cardiol* 2018, **113**(2):18.
12. Captur G, Manisty C, Moon JC: **Cardiac MRI evaluation of myocardial disease**. *Heart* 2016, **102**(18):1429-1435.
13. Ertl G, Frantz S: **Healing after myocardial infraction**. *Cardiovasc Res* 2005, **66**(1):22-32.
14. Saeed M, Liu H, Liang CH, Wilson MW: **Magnetic resonance imaging for characterizing myocardial diseases**. *Int J Cardiovasc Imaging* 2017, **33**(9):1395-1414.
15. Phelps ME: **PET: The merging of biology and imaging into molecular imaging**. *J Nucl Med* 2000, **41**(4):661-681.
16. Gaemperli O, Saraste A, Knuuti J: **Cardiac hybrid imaging**. *Eur Heart J-Cardiovasc Imaging* 2012, **13**(1):51-60.
17. Schinkel AFL, Bax JJ, Poldermans D, Elhendy A, Ferrari R, Rahimtoola SH: **Hibernating myocardium: Diagnosis and patient outcomes**. *Curr Probl Cardiol* 2007, **32**(7):375-410.
18. Hoogeveen RM, Nahrendorf M, Riksen NP, Netea MG, de Winther MPJ, Lutgens E, Nordestgaard BG, Neidhart M, Stroes ESG, Catapano AL: **Monocyte and haematopoietic progenitor reprogramming as commonmechanism underlying chronic inflammatory and cardiovascular diseases**. *Eur Heart J* 2018, **39**(38):3521-+.
19. Thackeray JT, Derlin T, Haghikia A, Napp LC, Wang Y, Ross TL, Schafer A, Tillmanns J, Wester HJ, Wollert KC: **Molecular imaging of the chemokine receptor CXCR4 after acute myocardial infarction**. *JACC-Cardiovasc Imag* 2015, **8**(12):1417-1426.
20. Lapa C, Reiter T, Werner RA, Ertl G, Wester HJ, Buck AK, Bauer WR, Herrmann K: **Ga-68 Pentixafor-PET/CT for imaging of chemokine receptor 4**

expression after myocardial infarction. *JACC-Cardiovasc Imag* 2015, **8**(12):1466-1468.

21. Narayanaswami V, Dahl K, Bernard-Gauthier V, Josephson L, Cumming P, Vasdev N: **Emerging PET radiotracers and targets for imaging of neuroinflammation in neurodegenerative diseases: outlook beyond TSPO**. *Mol Imaging* 2018, **17**:25.
22. Whitaker J, Tschabrunn CM, Jang J, Leshem E, O'Neill M, Manning WJ, Anter E, Nezafat R: **Cardiac MR characterization of left ventricular remodeling in a swine model of infarct followed by reperfusion**. *J Magn Reson Imaging* 2018, **48**(3):808-817.
23. Le-Petross HT, Cristofanilli M, Carkaci S, Krishnamurthy S, Jackson EF, Harrell RK, Reed BJ, Yang WT: **MRI features of inflammatory breast cancer**. *Am J Roentgenol* 2011, **197**(4):769-776.
24. Flogel U, Ding Z, Hardung H, Jander S, Reichmann G, Jacoby C, Schubert R, Schrader J: **In vivo monitoring of inflammation after cardiac and cerebral ischemia by fluorine magnetic resonance imaging**. *Circulation* 2008, **118**(2):140-148.
25. Nahrendorf M, Sosnovik D, Chen JW, Panizzi P, Figueiredo JL, Aikawa E, Libby P, Swirski FK, Weissleder R: **Activatable magnetic resonance imaging agent reports myeloperoxidase activity in healing infarcts and noninvasively detects the antiinflammatory effects of atorvastatin on ischemia-reperfusion injury**. *Circulation* 2008, **117**(9):1153-1160.
26. Sosnovik DE, Nahrendorf M, Weissleder R: **Molecular magnetic resonance imaging in cardiovascular medicine**. *Circulation* 2007, **115**(15):2076-2086.
27. Liu L, Alizadeh K, Donnelly SC, Dassanayake P, Hou TT, McGirr R, Thompson RT, Prato FS, Gelman N, Hoffman L *et al*: **MagA expression attenuates iron export activity in undifferentiated multipotent P19 cells**. *PLoS One* 2019, **14**(6):e0217842.
28. Fleming RE, Ponka P: **Iron Overload in Human Disease**. *N Engl J Med* 2012, **366**(4):348-359.

29. Madsen E, Gitlin JD: **Copper and iron disorders of the brain**. *Annu Rev Neurosci* 2007, **30**:317-337.
30. Anderson CP, Shen M, Eisenstein RS, Leibold EA: **Mammalian iron metabolism and its control by iron regulatory proteins**. *Biochim Biophys Acta-Mol Cell Res* 2012, **1823**(9):1468-1483.
31. Lane DJR, Merlot AM, Huang MLH, Bae DH, Jansson PJ, Sahni S, Kalinowski DS, Richardson DR: **Cellular iron uptake, trafficking and metabolism: Key molecules and mechanisms and their roles in disease**. *Biochim Biophys Acta-Mol Cell Res* 2015, **1853**(5):1130-1144.
32. Yanatori I, Kishi F: **DMT1 and iron transport**. *Free Radic Biol Med* 2019, **133**:55-63.
33. Donovan A, Lima CA, Pinkus JL, Pinkus GS, Zon LI, Robine S, Andrews NC: **The iron exporter ferroportin/Slc40a1 is essential for iron homeostasis**. *Cell Metab* 2005, **1**(3):191-200.
34. Lakhal-Littleton S, Wolna M, Carr CA, Miller JJJ, Christian HC, Ball V, Santos A, Diaz R, Biggs D, Stillion R: **Cardiac ferroportin regulates cellular iron homeostasis and is important for cardiac function**. *Proc Natl Acad Sci U S A* 2015, **112**(10):3164-3169.
35. Iwai K: **Regulation of cellular iron metabolism: Iron-dependent degradation of IRP by SCFFBXL5 ubiquitin ligase**. *Free Radic Biol Med* 2019, **133**:64-68.
36. Anderson GJ, Darshan D, Wilkins SJ, Frazer DM: **Regulation of systemic iron homeostasis: how the body responds to changes in iron demand**. *Biometals* 2007, **20**(3-4):665-674.
37. Knutson MD, Vafa MR, Haile DJ, Wessling-Resnick M: **Iron loading and erythrophagocytosis increase ferroportin 1 (FPN1) expression in J774 macrophages**. *Blood* 2003, **102**(12):4191-4197.
38. Ganz T: **Systemic iron homeostasis**. *Physiol Rev* 2013, **93**(4):1721-1741.
39. Delaby C, Pilard N, Puy H, Canonne-Hergaux F: **Sequential regulation of ferroportin expression after erythrophagocytosis in murine macrophages: early mRNA induction by haem, followed by iron-dependent protein expression**. *Biochem J* 2008, **411**:123-131.

40. Marro S, Chiabrando D, Messana E, Stolte J, Turco E, Tolosano E, Muckenthaler MU: **Heme controls ferroportin1 (FPN1) transcription involving Bach1, Nrf2 and a MARE/ARE sequence motif at position-7007 of the FPN1 promoter**. *Haematologica-the Hematology Journal* 2010, **95**(8):1261-1268.

41. Lymboussaki A, Pignatti E, Montosi G, Garuti C, Haile DJ, Pietrangelo A: **The role of the iron responsive element in the control of ferroportin1/IREG1/MTP1 gene expression**. *Journal of Hepatology* 2003, **39**(5):710-715.

42. Haschka D, Petzer V, Kocher F, Tschurtschenthaler C, Schaefer B, Seifert M, Sopper S, Sonnweber T, Feistritzer C, Arvedson TL: **Classical and intermediate monocytes scavenge non-transferrin-bound iron and damaged erythrocytes**. *JCI Insight* 2019, **4**(8):23.

43. Nemeth E, Tuttle MS, Powelson J, Vaughn MB, Donovan A, Ward DM, Ganz T, Kaplan J: **Hepcidin regulates cellular iron efflux by binding to ferroportin and inducing its internalization**. *Science* 2004, **306**(5704):2090-2093.

44. Qiao B, Sugianto P, Fung E, del-Castillo-Rueda A, Moran-Jimenez MJ, Ganz T, Nemeth E: **Hepcidin-induced endocytosis of ferroportin is dependent on ferroportin ubiquitination**. *Cell Metab* 2012, **15**(6):918-924.

45. Zhang DL, Rouault TA: **How does hepcidin hinder ferroportin activity?** *Blood* 2018, **131**(8):840-842.

46. Babitt JL, Huang FW, Wrighting DM, Xia Y, Sidis Y, Samad TA, Campagna JA, Chung RT, Schneyer AL, Woolf CJ: **Bone morphogenetic protein signaling by hemojuvelin regulates hepcidin expression**. *Nature Genet* 2006, **38**(5):531-539.

47. Hentze MW, Muckenthaler MU, Galy B, Camaschella C: **Two to tango: regulation of mammalian iron metabolism**. *Cell* 2010, **142**(1):24-38.

48. Park CH, Valore EV, Waring AJ, Ganz T: **Hepcidin, a urinary antimicrobial peptide synthesized in the liver**. *J Biol Chem* 2001, **276**(11):7806-7810.

49. Nairz M, Dichtl S, Schroll A, Haschka D, Tymoszuk P, Theurl I, Weiss G: **Iron and innate antimicrobial immunity-depriving the pathogen, defending the host**. *J Trace Elem Med Biol* 2018, **48**:118-133.

50. Wrighting DM, Andrews NC: **Interleukin induces hepcidin expression through STAT3**. *Blood* 2006, **108**(9):3204-3209.
51. Falzacappa MVV, Spasic MV, Kessler R, Stolte J, Hentze MW, Muckenthaler MU: **STAT3 mediates hepatic hepcidin expression and its inflammatory stimulation**. *Blood* 2007, **109**(1):353-358.
52. Theurl I, Theurl M, Seifert M, Mair S, Nairz M, Rumpold H, Zoller H, Bellmann-Weiler R, Niederegger H, Talasz H: **Autocrine formation of hepcidin induces iron retention in human monocytes**. *Blood* 2008, **111**(4):2392-2399.
53. Risko P, Platenik J, Buchal R, Potockova J, Kraml PJ: **The labile iron pool in monocytes reflects the activity of the atherosclerotic process in men with chronic cardiovascular disease**. *Physiol Res* 2017, **66**(1):49-61.
54. Haacke EM, Brown RW, Thompson MR, Venkatesan R: **Magnetic resonance imaging: physical principles and sequence design**, vol. 82.
55. Patel S, Patel S, Jadav H, Makwana K: **Role of MRI T2* imaging in evaluation of liver and cardiac iron overload, its correlation with serum ferritin and cardiac 2D echo correlation**. *J Evol Med Dent Sci-JEMDS* 2018, **7**(4):462-466.
56. Westwood M, Anderson LJ, Firmin DN, Gatehouse PD, Charrier CC, Wonke B, Pennell DJ: **A single breath-hold multiecho T2*cardiovascular magnetic resonance technique for diagnosis of myocardial iron overload**. *J Magn Reson Imaging* 2003, **18**(1):33-39.
57. Carpenter JP, He TG, Kirk P, Roughton M, Anderson LJ, de Noronha SV, Sheppard MN, Porter JB, Walker JM, Wood JC: **On T2*Magnetic Resonance and Cardiac Iron**. *Circulation* 2011, **123**(14):1519-1528.
58. Maekawa Y, Anzai T, Yoshikawa T, Asakura Y, Takahashi T, Ishikawa S, Mitamura H, Ogawa S: **Prognostic significance of peripheral monocytosis after reperfused acute myocardial infarction: A possible role for left ventricular remodeling**. *J Am Coll Cardiol* 2002, **39**(2):241-246.
59. Sasaki Y, Shimonaka Y, Ikuta K, Hosoki T, Sasaki K, Torimoto Y, Kanada H, Moriguchi Y, Kohgo Y: **Hepcidin production in response to iron is controlled by monocyte-derived humoral factors**. *Int J Hematol* 2014, **99**(1):12-20.

60. Andriopoulos B, Pantopoulos K: **Hepcidin generated by hepatoma cells inhibits iron export from co-cultured THP1 monocytes**. *Journal of Hepatology* 2006, **44**(6):1125-1131.

61. Canonne-Hergaux F, Donovan A, Delaby C, Wang HJ, Gros P: **Comparative studies of duodenal and macrophage ferroportin proteins**. *Am J Physiol-Gastroint Liver Physiol* 2006, **290**(1):G156-G163.

Chapter 2

2.1 Introduction

During an inflammatory response, circulating peripheral blood monocytes are recruited to the inflammation site by receptor-mediated interactions with chemokines. This monocyte activation leads to interactions with cell adhesion molecules on the activated endothelium and extravasation into target tissue [1]. Moreover, an increase in monocyte-related chemokines during inflammation leads to monocyte proliferation, directly correlating to an increase in the total number of monocytes [1]. Due to these inflammation-related chemokines, monocytes are one of the major immune cell types involved in chronic inflammatory conditions like atherosclerosis and heart failure. Furthermore, an increase in different monocyte sub-populations during pro- and anti-inflammatory stages may serve as markers for monitoring chronic inflammatory conditions [2, 3].

During an inflammatory response, monocytes play a vital role in host defense mechanisms against pathogens by limiting the availability of iron required for bacterial growth. This is facilitated by upregulation of the endocrine hormone hepcidin [4]. During inflammation, hepcidin binds to the iron export protein FPN and induces its internalization and degradation, thereby increasing iron retention in monocytes and macrophages [5]. Monocytes are the precursors of macrophages, which can be divided into at least two categories: M1 (pro-inflammatory) and M2 (anti-inflammatory) macrophages. While there is a spectrum of macrophage phenotypes, in general, M1 displays an iron storage phenotype while M2 exhibits an iron recycling phenotype [6]. These features of iron metabolism may allow us to differentiate between pro- and anti-inflammatory stages using MRI.

MRI is a noninvasive imaging modality that has been used to track cellular activities during inflammation [7, 8]. Iron-based contrast agents like superparamagnetic iron oxide particles have been developed to enhance image contrast and improve the tracking of inflammatory cells [7]. Since monocytes and macrophages are phagocytes, they internalize these exogenous contrast-enhancing particles thereby promoting more efficient tracking of these cells using MRI [7]. However, apart from phagocytic activity,

the effect of inflammation-associated changes in iron metabolism on the cellular MR signal have not been reported. In our study, we used the human monocyte THP-1 cell line to examine the endogenous cellular MR signal, varying extracellular iron and hepcidin to mimic the response to tissue injury (hemorrhage) and pro-inflammatory signaling [9], respectively.

2.2 Materials and Methods

2.2.1 Reagents

Unless otherwise indicated, the reagents were purchased from Thermo Fisher Scientific, Mississauga, Canada and from Sigma-Aldrich, Oakville, Canada.

2.2.2 THP-1 monocyte model

Human THP-1 monocytes, derived from the peripheral blood of a male acute monocytic leukemia patient (ATCC TIB-202), were cultured as a cell suspension in RPMI-1640 medium /10% fetal bovine serum /4 U/ml penicillin/4 µg/ml streptomycin/50 µM 2-mercaptoethanol. Cells were incubated at 37˚C in a 5% CO_2/air mixture. Cultures were maintained between 2-8 × 10^5 cells/ml based on cell counts determined through hemocytometry.

2.2.3 Iron supplementation

THP-1 cells were resuspended at a concentration of 2–4x10^5 cells/ml and cultured in the absence (-Fe) or presence (+Fe) of iron-supplemented medium containing 25µM ferric nitrate for 7 days (Figure 5A). Iron-supplemented cells were then returned to non-supplemented medium and cultured for an additional 1 (1h-Fe), 2 (2h-Fe), 4 (4h-Fe), and 24 (24h-Fe) hours (Figure 5B). At each time point, cells were collected in 850 µl radioimmunoprecipitation assay buffer (RIPA; 10 mM Tris-HCl pH 7.5/140 mM NaCl/1% NP-40/1% sodium deoxycholate/0.1% sodium dodecyl sulfate [SDS]) containing 150 µl Complete Mini protease inhibitor cocktail (Roche Diagnostic Systems, Laval, Canada) for protein analysis.

2.2.4 Hepcidin treatment

To examine the response of THP-1 monocytes to hepcidin, cells were cultured in the presence and absence of iron supplement, as described above, and in the presence of 200 ng/ml hepcidin for up to 24 hours (Figures 5C and 5D). Following hepcidin treatment, cells were prepared for protein analysis, elemental iron analysis or MRI.

For MRI experiments, THP-1 monocytes subjected to different iron treatment conditions in the presence and absence of hepcidin were collected intact by centrifugation at 300×g and 15˚C for 5 minutes. After centrifugation medium was removed and cells were washed three times with phosphate buffered saline pH 7.4 (PBS), cells were then centrifuged at 300 × g at 15˚C for 5 minutes in custom made Ultem wells (inner diameter: 4 mm; height: 10 mm, Lawson Imaging Prototype Lab). Once the cells were loaded into the Ultem wells, MRI relaxation rates were measured as described in section 2.2.8.

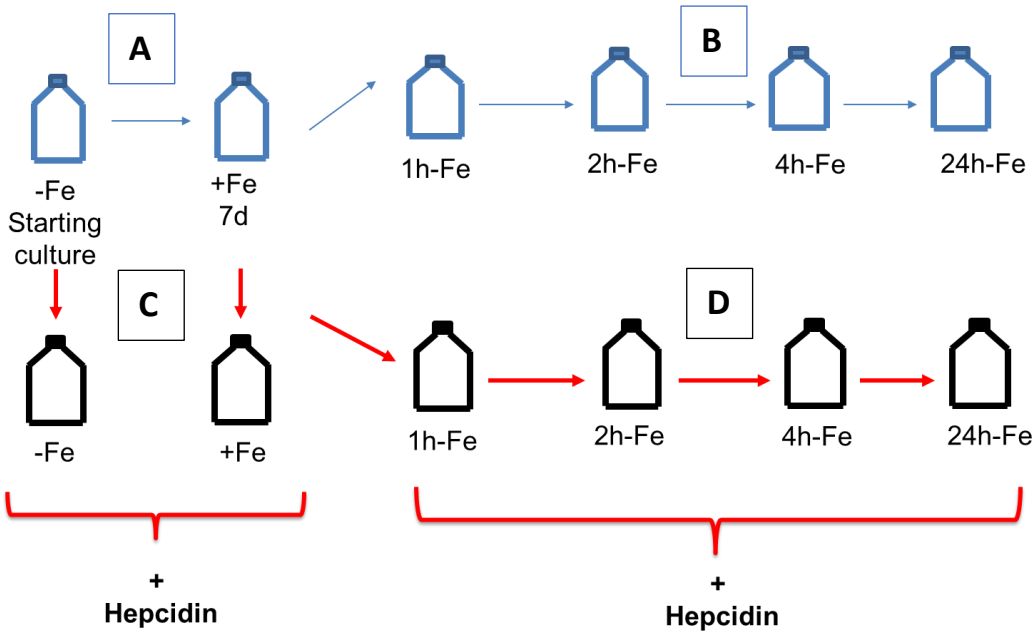

Figure 5. THP-1 cell treatments for Western blot and MRI. Cells were cultured in the absence (-Fe) or presence (+Fe) of iron supplementation (25 µM ferric nitrate/medium) for 7 days (**A**) and then harvested either immediately (-Fe and +Fe) or 1 (1h-Fe), 2 (2h-Fe), 4 (4h-Fe) and 24 (24h-Fe) hours after removal of extracellular iron supplement (**B**). Similarly, cultured cells were treated with 200 ng/ml hepcidin for up to 24 hours of culture prior to harvest (**C** and **D**).

2.2.5 Protein preparation and bicinchoninic acid assay

For Western blots and elemental iron analysis, cells cultured under different conditions (Figure 5) were centrifuged at 300 x g for 5 mins at 15°C. The supernatant was discarded, and the cell pellet was collected in 850 µL RIPA buffer with 150 µL Complete Mini protease inhibitor cocktail. Samples were placed on ice and complete cell lysis was achieved by sonicating three rounds, each for 12 seconds using the Sonic Dismembrator 500 (Fischer Scientific, Pittsburg, USA). Protein concentrations were determined using the bicinchoninic acid assay (BCA) with bovine serum albumin (BSA) as the protein standard [10].

2.2.6 Western blot

Samples containing total cellular protein, described in sections 2.2.3 and 2.2.4, were separated by SDS polyacrylamide gel electrophoresis (SDS-PAGE) according to published procedures [11]. Samples were assessed under reducing conditions using 1 mM dithiothreitol. Each sample contained 20 µg protein and was separated based on protein size using a 5% stacking gel and a 10% running gel. Molecular weight (M.W.) standards were run alongside protein samples for size comparison.

Separated protein was transferred to a nitrocellulose blot (iBlot Gel Transfer Stacks) following the manufacturer's protocol and published procedures [12]. To block nonspecific binding, the blot was incubated in 6% BSA/10 mM Tris HCl pH 7.4/0.9% NaCl buffered saline (Tris buffered saline, TBS)/0.02% sodium azide (TBSA) for a minimum of 2 hours at room temperature. To check for expression of FPN protein, the blot was incubated overnight at room temperature in 1:2000 rabbit anti-FPN /3%BSA/TBSA. After incubation with primary antibody, blots were washed for 30 minutes with 4 changes of TBS/0.1% Tween 20 (TBST) and then incubated for 2 hours at room temperature in 1:10,000 horseradish peroxidase (HRP)-conjugated goat anti-rabbit immunoglobulin (Ig) /1% BSA/TBS. After incubation in secondary antibody, blots were washed with TBST for 30 minutes with two changes of buffer. Bands were developed using the SuperSignal West Pico Chemiluminescent Substrate, detecting signal with the

ChemiDoc® Imaging System (Syngene, Fredrick, USA). The M.W. of FPN is approximately 63 kDa [13].

FPN expression was compared to the glyceraldehyde-3-phosphate dehydrogenase (GAPDH) control. Blots were stripped in solution containing 245 mM β-mercaptoethanol/2% SDS/62.5 mM tris-hydrochloric acid (pH6.8) and reprobed as described above, using 1:2000 rabbit anti-GAPDH as the primary antibody. The M.W. of GAPDH is approximately 37 kDa.

Expression of FPN was analyzed by densitometry using ImageJ software. The signal intensity of FPN was normalized to the signal intensity of GAPDH.

2.2.7 Trace elemental iron analysis

For elemental iron analysis, samples containing 2–4 mg/ml protein were prepared as indicated in section 2.2.5. The amount of iron in each sample was measured using inductively-coupled plasma mass spectrometry (ICP-MS, Biotron Analytical Services, Western University) and reported as total cellular iron content normalized to total amount of protein.

2.2.8 MRI phantoms

Each sample consisted of approximately 40–50 million cells placed in an Ultem well prior to mounting in a 9 cm, spherical 4% gelatin (porcine type A)/PBS phantom (Figure 6A) [14]. Cell phantoms were scanned at 3T on a Biograph mMR (Siemens AG, Erlangen, Germany) using previously developed sequences to acquire relaxation rates [14]. Single echo spin echo and multi-echo gradient echo sequences were applied to obtain R_2 and R_2*, respectively. R_2' was calculated by subtraction (R_2* - R_2) [14]. The following imaging parameters were used for MR image acquisition. For R_1, longitudinal relaxation rate, an inversion recovery spin echo sequence was used. The slice thickness was 3 mm (Figure 6B), the field of view was 120 × 120 mm, matrix size was 128 × 128 mm, voxel size was: 3.0 × 0.9 × 0.9 mm^3, repetition time (TR) was: 4000 ms, flip angle

was 90˚, inversion times were 22, 200, 500, 1000, 2000 and 3900 ms and echo time (TE) was 13 ms. For both single echo spin echo and multi-echo gradient echo sequences, slice thickness was 3 mm (Figure 6B), the field of view was 120 × 120 mm, matrix size was 192 × 192 mm and voxel size was 3.0 × 0.6 × 0.6 mm^3. For the single echo spin echo sequence, TEs were 13, 20, 25, 30, 40, 60, 80, 100, 150, 200 ms; TR was 2010 ms; flip angle was 90˚; and scanning time was approximately 61 minutes. For multi-echo gradient echo, TEs were 6.12, 14.64, 23.16, 31.68, 40.2, 50, 60, 70, 79.9 ms; TR was 200 ms; flip angle was 60˚ and scanning time was approximately 25 minutes.

Transverse relaxation rates (R_2* and R_2) were measured using software developed in Matlab 7.9.0 (R2010b). This software was used to determine the region of interest (ROI) when measuring R_2* and R_2 signals. The ROI included 21 voxels within the sample, avoiding the wall of the well. Relaxation rates were calculated using the average signal intensity and least-squares curve fitting. Relaxation rates were reported as the mean +/- standard error of the mean (SEM) using GraphPad Prism software, version 8.0.0.

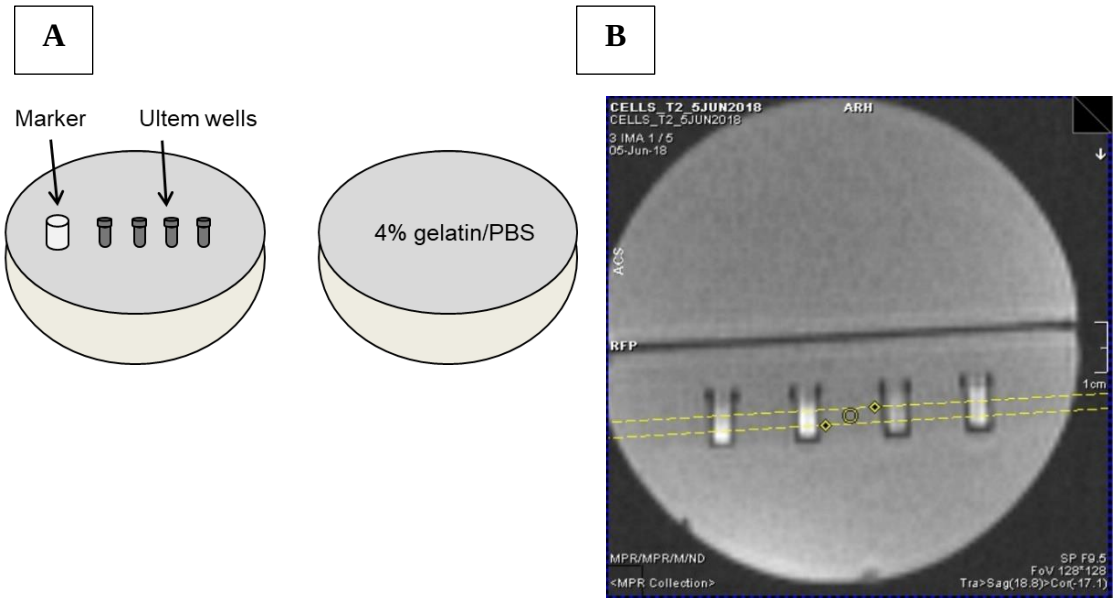

Figure 6. MRI gelatin phantom and slice localization. A. Cells in Ultem wells were mounted in one hemisphere of a 9 cm spherical phantom and overlaid with 4% gelatin/PBS. In the final assembly, this hemisphere was secured to a gelatin-only hemisphere to give the overall 9 cm sphere. A plastic marker was used as an indicator of sample layout [14]. **B.** To acquire MR images, the cell phantom was placed in a knee coil. Yellow lines in the locator image indicate the 3 mm slice thickness through the samples.

2.2.9 Statistical analysis

Statistical analyses were performed using SPSS, version 25. MR relaxation rates obtained for treatment time points, reflecting changes in extracellular iron supplementation or hepcidin treatment, were analyzed using one-way analysis of variance (ANOVA). Significant differences were defined by $p < 0.05$. To test the effect of the combination of hepcidin and iron supplementation on MR relaxation rates, two-way ANOVA was conducted to determine significant differences. Pearson's correlations were assessed to determine the relationship between total cellular iron content and MR relaxation rate. A linear regression model was applied using cellular iron content as the independent variable and MR relaxation rate as the dependent variable to obtain the line of best fit.

2.3 Results

2.3.1 Effect of iron and hepcidin on FPN expression

To obtain evidence of iron export activity in THP-1 monocytes, cultured cells were incubated in the presence and absence of iron supplementation. Western blots revealed FPN expression in all samples (Figure 7A). Under standard culture conditions (-Fe), THP-1 cells express maximal levels of iron export protein, similar to the level of GAPDH expression (ratio ~1 in Figure 7C). Moreover, after 7 days of iron supplementation (+Fe), there is little or no change in the expression of FPN, as confirmed by densitometry (Figure 7C, blue bars). However, up to two hours after the withdrawal of iron supplement, FPN expression significantly declines (+Fe versus 1h-Fe, $p < 0.01$; +Fe versus 2h-Fe, $p < 0.01$), before significantly recovering at 4 hours after the withdrawal of extracellular iron (2h-Fe versus 4h-Fe, $p < 0.05$; Figures 7A and 7C, blue bars). After 24 hours of iron supplement withdrawal (24h-Fe), FPN expression significantly decreases (+Fe versus 24h-Fe and 4h-Fe versus 24h-Fe, $p < 0.001$)

To determine the effect of the polypeptide hormone hepcidin on FPN expression, cells were treated with exogenous hepcidin (Figure 7B). Potential changes in FPN expression in response to hepcidin were assessed using the Western blot to track protein degradation. One-way ANOVA suggests FPN expression significantly decreases (Figure 7C) at 4 and 24 hours of iron supplement withdrawal in hepcidin-treated samples (+Fe orange versus 4h-Fe orange, $p < 0.01$; +Fe orange verses 24h-Fe orange, $p < 0.05$).

Two-way ANOVA comparing hepcidin treated and untreated samples (red lines) indicates that at baseline (-Fe), FPN expression was significantly decreased in response to hepcidin (-Fe blue verses -Fe orange, $p < 0.001$), confirming a biologically meaningful interaction. Also, in the +Fe sample, FPN expression indicates a significant decrease (+Fe blue versus +Fe orange, $p < 0.001$). Interestingly, one hour after the removal of iron supplement and hepcidin treatment (1h-Fe), FPN is still expressed at a low level, suggesting little influence of exogenous hepcidin. This decreases even further after 4 hours of iron supplement withdrawal (4h-Fe blue versus 4h-Fe orange, $p < 0.001$) suggesting that FPN expression is down-regulated in the presence of hepcidin at these timepoints.

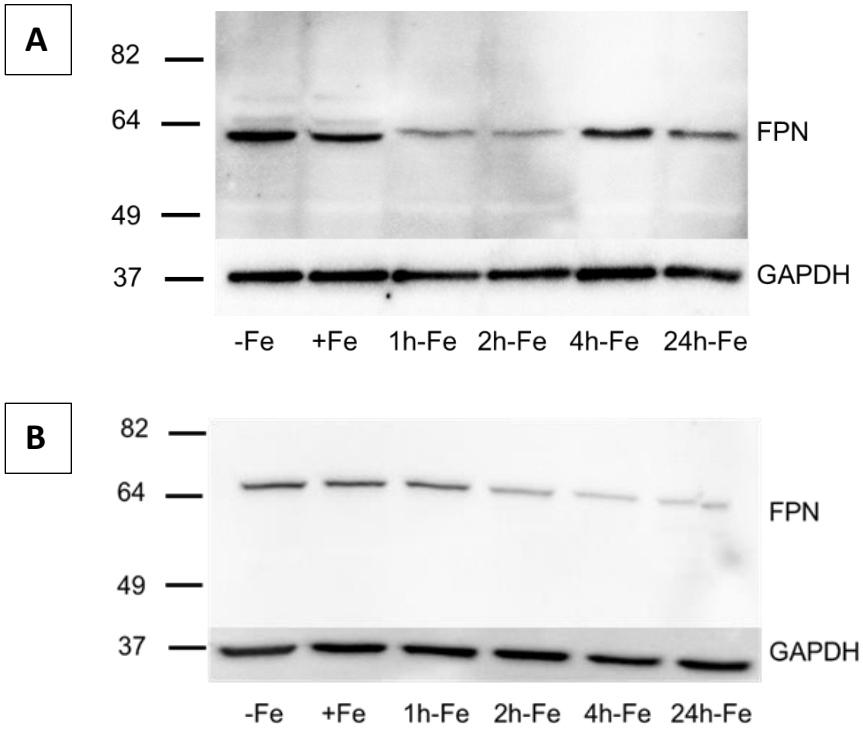
A
82
64
49
37
FPN
GAPDH
-Fe
+Fe
1h-Fe
2h-Fe
4h-Fe
24h-Fe
B
82
64
49
37
FPN
GAPDH
-Fe
+Fe
1h-Fe
2h-Fe
4h-Fe
24h-Fe
C
FPN
GAPDH
1.5
1.0
0.5
0.0
No Hepcidin
Hepcidin
-Fe
+Fe
1h-Fe
2h-Fe
4h-Fe
24h-Fe

Figure 7. Regulation of ferroportin (FPN) expression in THP-1 monocytes by extracellular iron and hepcidin. THP-1 cells were cultured for 7 days in the absence (-Fe) or presence (+Fe) of iron-supplemented medium containing 25 μM ferric nitrate. Cells were either harvested immediately or after the withdrawal of iron supplement and culture for an additional 1 (1h-Fe), 2 (2h-Fe), 4 (4h-Fe) and 24 (24h-Fe) hours. To examine FPN regulation, -Fe and +Fe samples were grown in the presence of 200 ng/ml hepcidin for the last 24 hours of culture while hepcidin was added to all other samples after the removal of iron supplement. Representative Western blots show the change in FPN expression in the absence (**A**) and presence (**B**) of hepcidin (refer to Appendix E for additional immunoblot results). Molecular weight standards are indicated on the left while GAPDH provided a loading control**.** Densitometry (**C**) indicates relative level of FPN expression normalized to GAPDH (n = 3 independent experiments, * $p < 0.05$, ** $p < 0.01$, *** $p < 0.001$).

2.3.2 Effect of hepcidin on cellular iron content

Despite changes in FPN expression, cellular iron content does not change significantly across all time points, regardless of changes in iron supplementation (Figure 8A). There was no correlation between the ratio of FPN/GAPDH and total cellular iron content. Elemental iron analysis using ICP-MS shows cellular iron content ranges between 0.175–0.679 µg/mg protein, indicating a modest rise in iron content and return to the baseline. However, in the presence of iron supplementation and hepcidin (+Fe) there is a significant increase ($p < 0.01$) in total cellular iron content (Figure 8B) compared to the baseline control (-Fe versus +Fe, $p < 0.01$). Subsequently, one hour after the withdrawal of iron supplement (1h-Fe), hepcidin treatment results in a significant decrease in total cellular iron content (+Fe versus 1h-Fe, $p < 0.05$, Figure 8B). Interestingly, two hours after the removal of iron supplement (2h-Fe), hepcidin treatment results in a second increase in total cellular iron content (1h-Fe versus 2h-Fe, $p < 0.001$) which is sustained up to 4h-Fe and then followed by a significant decrease in cellular iron content (4h-Fe versus 24h-Fe, $p < 0.01$). These data reflect a biphasic response of THP-1 cells to hormonal treatment with hepcidin.

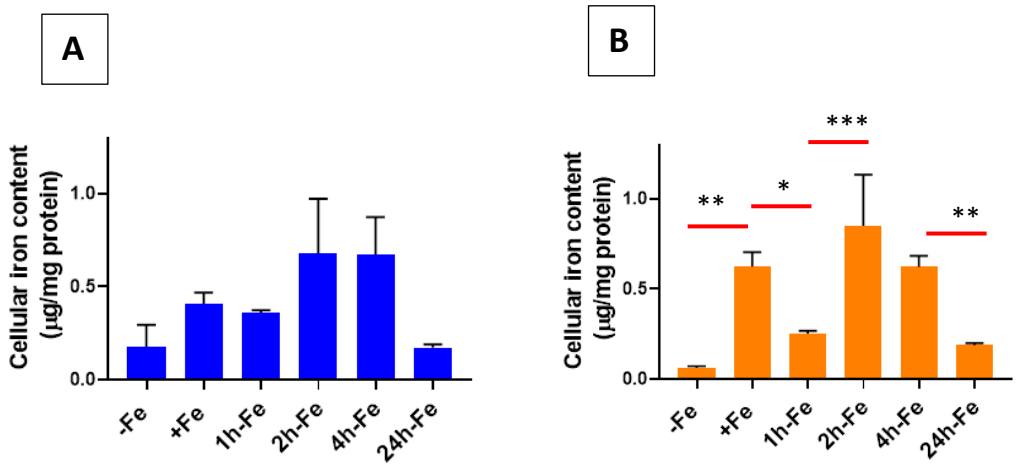

Figure 8. Influence of extracellular iron and hepcidin on intracellular iron content. To examine the effect of changes in extracellular iron (**A**), THP-1 cells were cultured for 7 days in the absence (-Fe) or presence (+Fe) of iron-supplemented medium containing 25 µM ferric nitrate. Cells were either harvested immediately (-Fe and +Fe) or after removal of iron supplement and culture for an additional 1 (1h-Fe), 2 (2h-Fe), 4 (4h-Fe) or 24 (24h-Fe) hours in non-supplemented medium. To examine the regulation of iron export (**B**), -Fe and +Fe samples were grown in the presence of 200 ng/ml hepcidin for the last 24 hours of culture while hepcidin was added to all other samples after the removal of iron supplement. Total cellular iron content was assessed by ICP-MS and was normalized to protein concentration. In response to changes in extracellular iron, the total intracellular iron content ranged between 0.175 and 0.679 µg/mg protein but was not significantly different between samples (n = 3-4). However, in the presence of hepcidin, iron-supplemented cells (+Fe) retained significantly more cellular iron than non-supplemented cells (-Fe) but returned to baseline values within 1 hour after the withdrawal of iron supplement. A biphasic response to the addition of hepcidin was observed between 2 and 24 hours after the withdrawal of iron supplement (2h-Fe to 24h-Fe; n = 3-4). * $p < 0.05$, ** $p < 0.01$, *** $p < 0.001$.

2.3.3 Effect of iron supplement on transverse relaxivities

To examine the effect of changes in extracellular iron on transverse relaxivity, THP-1 monocytes were mounted in an MR phantom and scanned at 3T. Mean transverse relaxation rate of these cells under different conditions of iron treatment indicates a relatively high signal (approximately $\geq$ 10 Sec^{-1}) for both the total transverse relaxation rate (R_2*, Figure 9A) and its irreversible component (R_2, Figure 9B). Neither R_2* nor R_2 was influenced by continuous iron supplementation (+Fe) compared to the control culture (-Fe). However, withdrawal of iron supplementation for 1 (1h-Fe) to 4 (4h-Fe) hours significantly increased the R_2* signal (+Fe versus 1h-Fe, $p < 0.01$; +Fe versus 2h-Fe, $p < 0.001$; +Fe versus 4h-Fe, $p < 0.01$). But, by 24 hours (24h-Fe), R_2* returned to baseline values (4h-Fe versus 24h-Fe, $p < 0.01$; Figure 9A).

The effect of iron supplement withdrawal on R_2 was not apparent for 4 hours (4h-Fe) at which point R_2 significantly increased over baseline values (-Fe versus 4h-Fe, $p < 0.05$) before returning to control levels (4h-Fe versus 24h-Fe, $p < 0.01$).

The R_2* signal is made up of two components: reversible R2′ and irreversible R2. Consistent with R_2* and R_2, the R_2' signal (Figure 9C) showed no significant change in the presence of iron supplementation (+Fe) compared to the control culture (-Fe). However, R_2' significantly increased 1 (1h-Fe) to 4 (4h-Fe) hours after iron supplement was withdrawn (+Fe versus 1h-Fe, $p < 0.01$; +Fe versus 2h-Fe, $p < 0.001$; +Fe versus 4h-Fe, $p < 0.05$). By 24 hours after the removal of iron supplement (24h-Fe), R_2' returned to baseline values (4h-Fe versus 24h-Fe, $p < 0.001$).

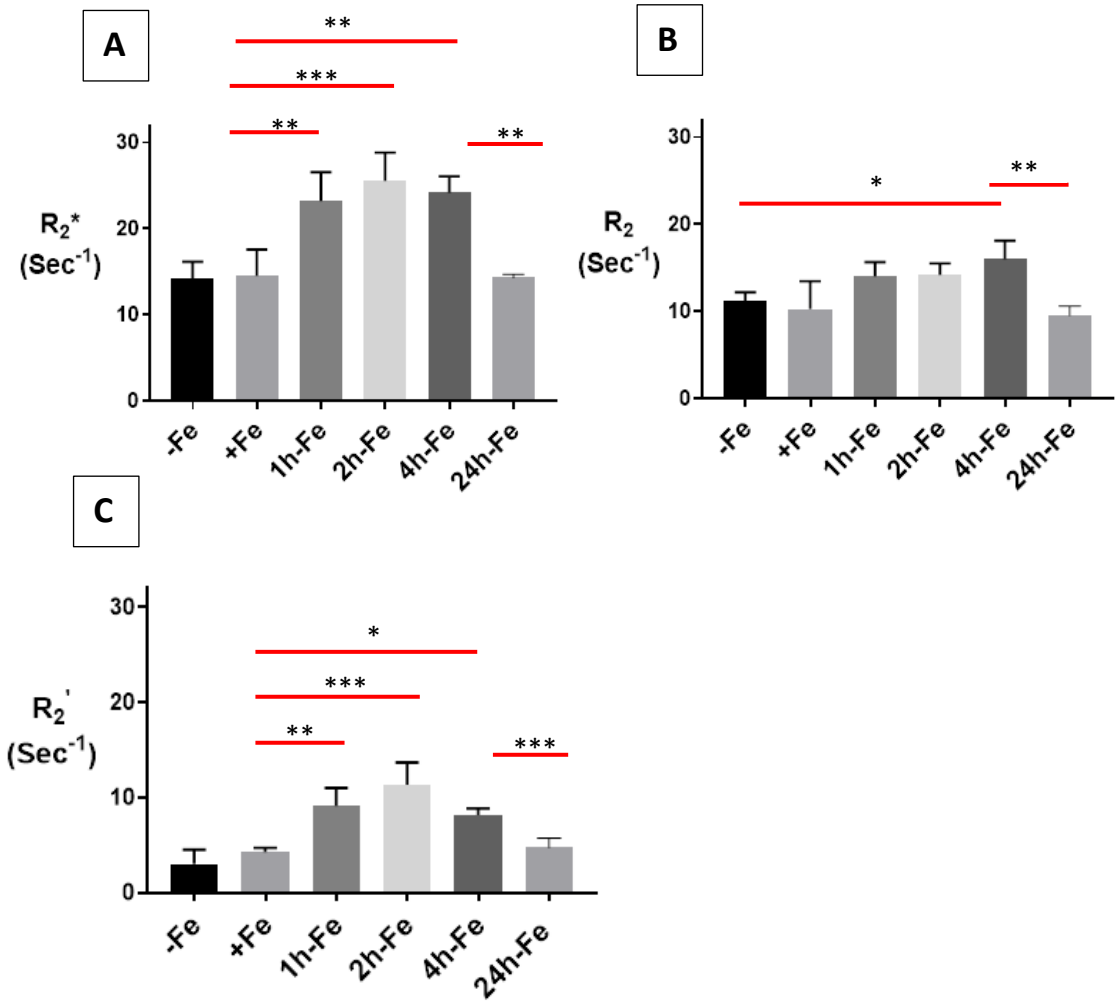

Figure 9. Influence of extracellular iron on transverse relaxation rates in human monocytes. To examine the influence of extracellular iron, THP-1 cells were cultured in the absence (-Fe) or in the presence (+Fe) of iron-supplemented medium containing 25 µM ferric nitrate for 7 days. Cells were then harvested and scanned either immediately (-Fe and +Fe) or cultured for an additional 1 (1h-Fe), 2 (2h-Fe), 4 (4h-Fe) and 24 (24h-Fe) hours after removal of extracellular iron supplement. One-way ANOVA indicates significant changes between samples subjected to iron treatments. **A.** Regardless of iron supplementation (+/- Fe), human THP-1 cells displayed relatively high transverse relaxation rates (R_2*). However, within an hour of iron supplement withdrawal, R_2* significantly increased and remained elevated up to 4 hours before returning to baseline.

B. The irreversible component of transverse relaxivity (R_2) is increased modestly at 4h-Fe before returning to baseline. **C.** Like R_2*, the reversible component ($R_2' = R_2^* - R_2$) increased significantly upon withdrawal of iron supplementation and also remained elevated up to 4 hours before returning to baseline (n = 3-4, * $p < 0.05$, ** $p < 0.01$, *** $p < 0.001$).

2.3.4 Effect of hepcidin on transverse relaxivities

THP-1 cells were incubated with various amounts of iron supplement and hepcidin before scanning at 3T to measure relaxation rates. The mean values of R_2*, R_2 and R_2' are shown in Figure 10. By adding hepcidin, we aimed to interrupt the iron export activity of monocytes. Total transverse relaxation rate (R_2*) significantly increased ($p < 0.05$) in the presence of iron supplementation and hepcidin (-Fe versus +Fe, Figure 10A) and remained high for 1 hour after withdrawing iron supplementation (+Fe versus 1h-Fe). However, 2 hours after iron supplementation withdrawal (2h-Fe) R_2* significantly increased again (1h-Fe versus 2h-Fe, $p < 0.001$) and remained high until 4 hours after iron supplement withdrawal when the signal returned to baseline (4h-Fe versus 24h-Fe, $p < 0.001$).

Under the same conditions, the irreversible component (R_2, Figure 10B) showed significant changes similar to R_2*.

The reversible component (R_2', Figure 10C) remained unchanged in the presence of iron supplement (+Fe) compared to the baseline (-Fe). However, R_2' significantly increased ($p < 0.01$) after 2 hours of iron withdrawal (-Fe versus 2h-Fe, $p < 0.01$; 1h-Fe versus 2h-Fe, $p < 0.01$) before returning to baseline (2h-Fe versus 24h-Fe, $p < 0.01$).

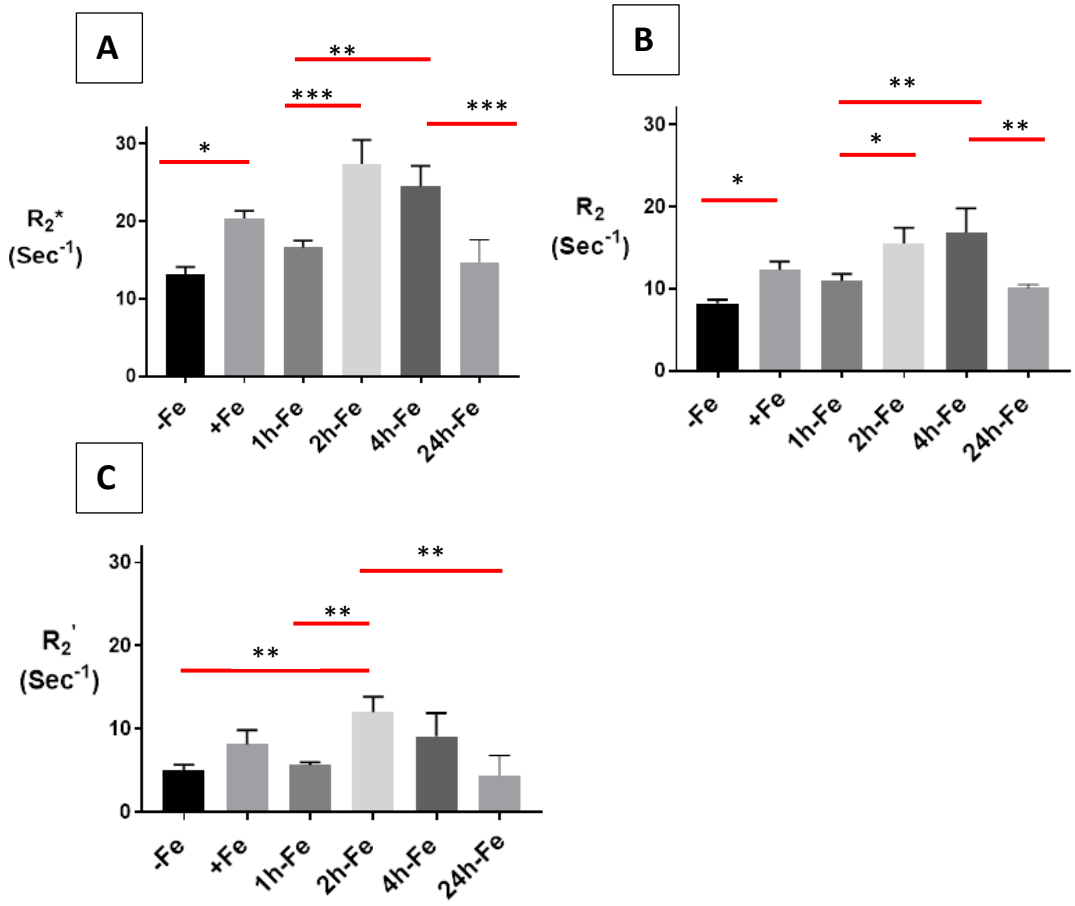

Figure 10. Influence of extracellular iron and hepcidin on transverse relaxation rates in human monocytes. To examine the influence of extracellular iron and hepcidin, THP-1 cells were cultured in the absence (-Fe) or in the presence of (+Fe) iron-supplemented medium containing 25 µM ferric nitrate for 7 days. Cells were harvested either immediately or 1 (1h-Fe), 2 (2h-Fe), 4 (4h-Fe) and 24 (24h-Fe) hours after removal of extracellular iron supplement. Also, -Fe and +Fe samples were grown in the presence of 200 ng/ml hepcidin for the last 24 hours of culture while hepcidin was added to all other samples after the removal of iron supplement. One-way ANOVA indicates significant changes between samples subjected to iron and hepcidin treatments. **A.** In the presence of iron supplementation (+Fe), human THP-1 cells display a significant increase in the total transverse relaxation rate (R_2*). For the first hour after iron supplement withdrawal, R_2* remains relatively constant. **B.** The irreversible component (R_2) also increased significantly in the presence of iron. **C**. The reversible component (R_2') was

only significantly increased two hours after iron supplement withdrawal. n = 3-4, * $p < 0.05$, ** $p < 0.01$, *** $p < 0.001$

2.3.5 Comparison of transverse relaxivities between hepcidin treated and untreated THP-1 cells.

The influence of hepcidin on THP-1 samples was evaluated using two-way ANOVA. Figure 11 indicates that in the presence of both hepcidin and various levels of extracellular iron, there are significant changes in relaxation rates. R_2* (Figure 11A) significantly increases ($p < 0.05$) in the presence of both extracellular iron and hepcidin (+Fe, orange bar) compared to monocytes treated with iron alone (+Fe, blue bar). R_2* also significantly decreases within 1 hour of iron supplement withdrawal (1h-Fe) in the presence of hepcidin (orange bar versus blue bar). There was no influence of exogenous hepcidin on R_2* at any other time point. Likewise, R_2 was not influenced by hepcidin (Figure 11B) under any of the conditions examined. A comparison between R_2' (Figure 11C) signals indicates that hepcidin predominantly influences the reversible component of transverse relaxation rate.

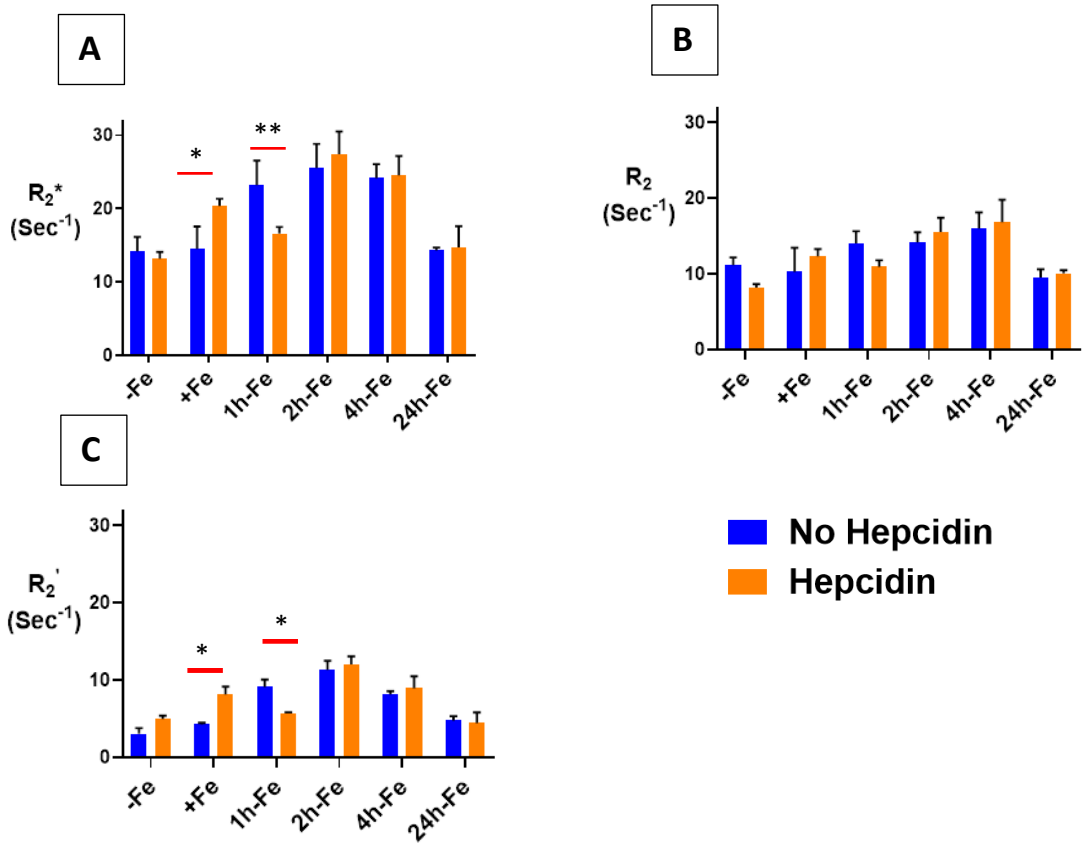

Figure 11. Influence of extracellular iron and hepcidin on transverse relaxation rates in human monocytes. To examine the influence of extracellular iron and hepcidin, THP-1 cells were cultured in the absence (-Fe) or in the presence of (+Fe) iron-supplemented medium containing 25 µM ferric nitrate for 7 days. These samples were treated with 200 ng/ml hepcidin for the last 24 hours of culture. Cells were harvested either immediately or 1 (1h-Fe), 2 (2h-Fe), 4 (4h-Fe) and 24 (24h-Fe) hours after removal of extracellular iron supplement. Also, these samples were treated with 200 ng/ml of hepcidin for up to 24 hours before the harvest. Two-way ANOVA indicates significant changes between samples treated in the presence and absence of hepcidin**.** Both R_2* (**A**) and R_2' (**C**) relaxation rates increase significantly in the presence of iron supplement and hepcidin, with a significant decrease within an hour of iron supplement withdrawal. The irreversible component R_2 (**B**) is not significantly influenced by hepcidin. n = 3-4, * $p < 0.05$, ** $p < 0.01$

2.3.6 Influence of iron supplement and hepcidin on longitudinal relaxivity

The R_1 signal remained constant across all treatment conditions and time points in samples without hepcidin (Figure 12A). However, in the presence of hepcidin (Figure 12B), longitudinal relaxation rate significantly increased upon iron supplementation (-Fe versus +Fe, $p < 0.01$) and remained elevated up to four hours after the removal of iron supplement. Comparison of hepcidin treatment using two-way ANOVA (Figure 12C) showed a significant decrease in R_1 ($p < 0.05$) at 1h-Fe in the presence of hepcidin. Regardless, there was no significant change in cellular iron content with and without hepcidin at 1h-Fe.

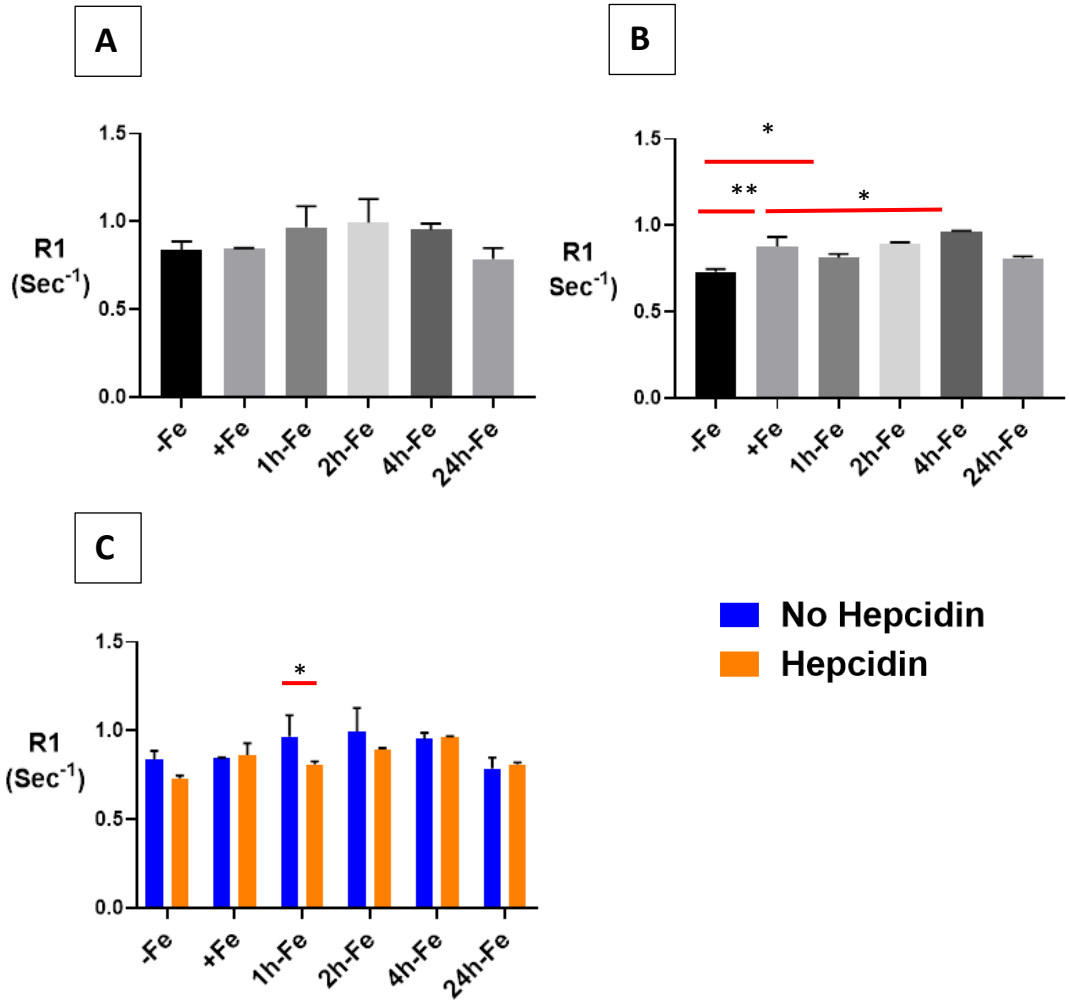

Figure 12. Influence of extracellular iron and hepcidin on longitudinal relaxation rates. To examine the influence of extracellular iron and hepcidin, THP-1 cells were cultured in the absence (-Fe) or presence (+Fe) of iron-supplemented medium containing 25 µM ferric nitrate for 7 days. These samples were treated with 200 ng/ml hepcidin for the last 24 hours of culture. Cells were harvested either immediately or 1 (1h-Fe), 2 (2h-Fe), 4 (4h-Fe) and 24 (24h-Fe) hours after removal of extracellular iron supplement. Also, these samples were treated with 200 ng/ml of hepcidin for up to 24 hours before the harvest. One-way ANOVA indicates, **A**. In the absence of hepcidin, R_1 remains relatively constant across all samples. **B.** In the presence of hepcidin, R_1 significantly increased following iron supplementation (+Fe) and remained elevated up to 4 hours after the withdrawal of iron supplement. Two-way ANOVA indicates, **C**. In the presence of hepcidin, there was a significant decrease in R_1 at 1h-Fe. n = 3, * $p < 0.05$, ** $p < 0.01$

2.3.7 Correlation between cellular iron content and transverse relaxivities

To understand the correlation between cellular iron content (the independent variable) and transverse relaxation rate (the dependent variable), Pearson's correlation test was performed. There was a moderate positive correlation (Figure 13A, $r = 0.62$, $p < 0.01$) between cellular iron content and the total transverse relaxation rate, R_2*; however, no correlation was obtained between cellular iron content and the irreversible R_2 component of transverse relaxation rate. In THP-1 monocytes, the moderate positive correlation (Figure 13B, $r = 0.61$, $p < 0.01$) between cellular iron content and transverse relaxivity rests with the reversible R_2' component. The lines of best fit were determined using a linear regression model and an independent samples t-test indicates these relationships have similar slopes, between 5.8 and 8.8.

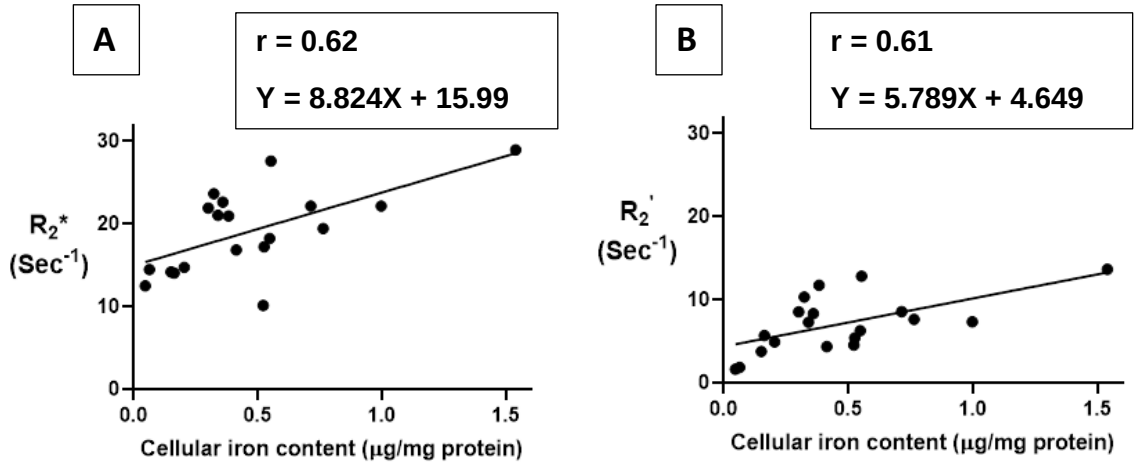

Figure 13. Influence of changes in extracellular iron on the correlation between cellular iron content and MR transverse relaxation rates. To examine the influence of extracellular iron, THP-1 cells were cultured in the absence (-Fe) or in the presence (+Fe) of iron-supplemented medium containing 25 µM ferric nitrate for 7 days. Cells were then harvested and scanned either immediately (-Fe and +Fe) or cultured an additional 1 (1h-Fe), 2 (2h-Fe), 4 (4h-Fe) and 24 (24h-Fe) hours after removal of extracellular iron supplement. Total cellular iron content was assessed by ICP-MS and was normalized to protein concentration. There is a moderate positive correlation between cellular iron content and both R_2* (**A**) and R_2' (**B**). For both graphs, n = 19 and $p < 0.01$.

For the samples treated with hepcidin, Pearson's correlation analysis shows a strong positive correlation between cellular iron content and R_2* (Figure 14A, $r = 0.80$, $p < 0.001$). Surprisingly, after THP-1 monocytes are treated with hepcidin, there is a moderate positive correlation between cellular iron content and both R_2 (Figure 14B, $r = 0.71$, $p < 0.01$) and R_2' (Figure 14C, $r = 0.75$, $p < 0.001$). Using a linear regression model, the lines of best fit were determined. An independent samples t-test indicates that the slopes of these lines are similar for all transverse relaxation rates. Moreover, comparison of the slopes between hepcidin treated and untreated samples revealed there were no significant changes in the slope when samples were exposed to hepcidin.

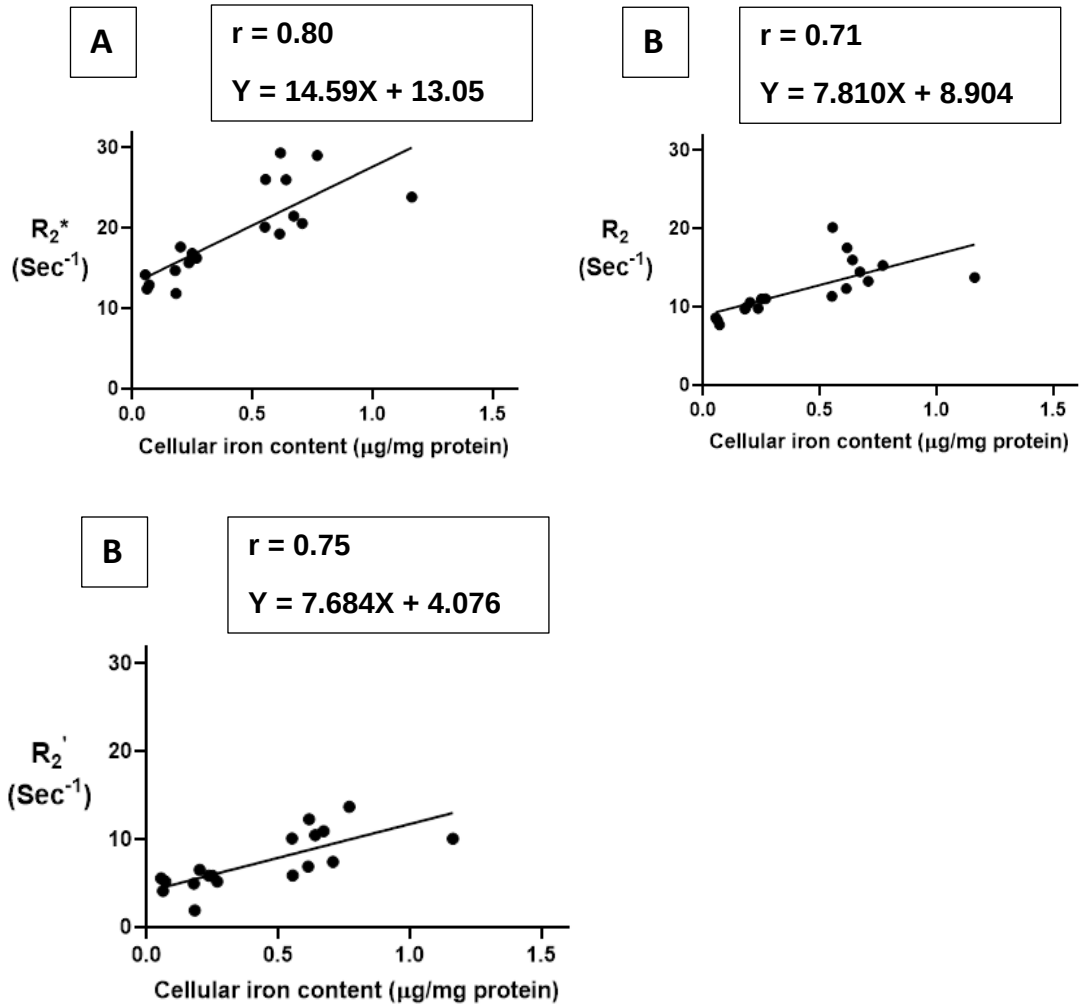

Figure 14. Influence of hepcidin on the correlation between cellular iron content and transverse relaxation rates. To examine the influence of extracellular iron and hepcidin, THP-1 cells were cultured in the absence (-Fe) or in the presence of (+Fe) iron-supplemented medium containing 25 µM ferric nitrate for 7 days. These samples were treated with 200 ng/ml hepcidin for the last 24 hours of culture. Cells were harvested either immediately or 1 (1h-Fe), 2 (2h-Fe), 4 (4h-Fe) and 24 (24h-Fe) hours after removal of extracellular iron supplement. Also, these samples were treated with 200 ng/ml of hepcidin for up to 24 hours before the harvest. The total cellular iron content was assessed by ICP-MS and normalized to protein concentration. **A.** There is a strong correlation between cellular iron content and R_2* ($p < 0.001$). **B**. There is a moderate

correlation between cellular iron content and R_2 ($p < 0.01$) **C.** There is also a moderate correlation between cellular iron content and R_2' ($p < 0.001$). n = 18

2.4 Discussion

Monocytes are the most abundant cell type during an inflammatory response [2]. As such, different monocyte subpopulations reflecting pro- and anti-inflammatory stages may potentially serve as biomarkers for monitoring inflammation. In our study, we used the human THP-1 monocytic cell line to monitor hepcidin-FPN interactions, which occur in only a few cell types and may provide a relatively unique biomarker for molecular imaging.

Iron export in monocytes

Hepcidin is a polypeptide hormone secreted in response to changes in systemic iron and pro-inflammatory cytokines like IL-6. Hepcidin activity downregulates the iron export protein, FPN. By culturing monocytes in the presence and absence of hepcidin (200 ng/ml), while treating the cells with extracellular iron supplementation (25 µM ferric nitrate), we investigated the influence of iron export on MR relaxation rates. In addition, we measured the cellular iron content and correlated it with MR relaxation rates to better understand the relationship between these measures.

As the main mammalian iron export protein, FPN recycles intracellular iron back to the plasma. FPN is only expressed by certain cells, predominantly hepatocytes, enterocytes, macrophages and their precursors - the monocytes [15]. In response to inflammation, monocytes phagocytose damaged red blood cells and then release the iron recovered from heme back into plasma, predominantly for the synthesis of new red blood cells [16]. As the expression of FPN is integral to this process, in our study, we confirmed that THP-1 monocytes express the iron export protein FPN (-Fe, Figure 7A). Relative to the housekeeping protein, GAPDH, the expression of FPN is abundant (ratio ~1, Figure 7C). These data are supported by literature related to FPN expression in freshly isolated human blood monocytes and THP-1 monocytes [17, 18]. Our observations of FPN expression in the presence of extracellular iron supplementation (+Fe, Figure 7A) are consistent with a study showing an increase in FPN mRNA levels in THP-1 cells under

iron supplemented conditions [19]. Given the relatively equal levels of FPN protein +/-Fe (by densitometry, Figure 7C), these findings further suggest that FPN turnover, through transcriptional and post-translational mechanisms, may both be active in monocytes, in the presence of an extracellular iron supplement. FPN protein expression was downregulated within 1 to 2 hours after the removal of iron supplement (Figure 7C), consistent with post-translational regulation of FPN and consistent with the reported production of hepcidin by THP-1 monocytes, which leads to FPN ubiquitination [16, 17]. This hypothesis implicates hepcidin autocrine/paracrine activity, which we documented upon withdrawal of iron supplementation (in the absence of exogenous hepcidin). We note that no further degradation of FPN by exogenously added hepcidin was obtained at 1h-Fe and 2h-Fe, as would be expected for autocrine/paracrine regulation.

Interestingly, FPN returns to baseline levels (high expression) by 4h-Fe only to drop again at 24h-Fe, indicating a biphasic response to (the presumed) monocyte self-regulation by hepcidin. The short-lived nature of the active form of hepcidin (hepcidin-25) permits fine-tuned control of FPN and therefore the iron export function of monocytes.

Hepcidin regulation of monocytes

When pro-inflammatory signaling through IL-6 promotes inflammation, the hormone hepcidin is produced by the liver [20, 21]. Through downregulation of FPN in monocytes and macrophages, hepcidin reduces the extracellular iron availability at the site of inflammation. Consequently, hepcidin helps fight infection since iron is a critical co-factor for many microbes [22, 23]. In our study, we detected downregulation of ferroportin expression in THP-1 monocytes in response to exogenous hepcidin treatment (Figure 7B) whenever monocyte self-regulation did not predominate: at baseline (-Fe), in the presence of continuous iron supplementation (mimicking hemorrhage, +Fe), and at 4h-Fe. Hence, monocytes appear to be subject to endocrine, paracrine and autocrine regulation by hepcidin [17].

Over the years, clinicians have been struggling to distinguish between pro-inflammatory and anti-inflammatory stages post-AMI to prevent unwanted tissue remodeling leading to

heart failure [24, 25]. Since monocytes along with hormones like hepcidin travel to the infarcted myocardium through systemic circulation post-AMI, we expected that pro-inflammatory signaling through hepcidin may cause increased iron retention in monocytes and facilitate their detection using MRI. In the absence of exogenous hepcidin (low/no endocrine signaling), total cellular iron content is not significantly altered by changes in extracellular iron (Figure 8A), pointing to the efficiency of autocrine/paracrine hepcidin-mediated regulation of iron homeostasis in an iron-exporting cell type. While this form of monocyte iron regulation does not influence R1, it is transiently detected by R_2* (Figure 9A) and specifically the reversible R_2' component (Figure 9C). Indeed, under these conditions, there was no correlation between iron and R_2; however, there was a moderate correlation between iron and both R_2* and R_2' (Figure 13). To the extent that R_2 represents protein-bound iron, it appears that autocrine/paracrine regulation of FPN largely influences the unbound iron fraction that modulates the R_2' signal.

Our examination of pseudo-endocrine regulation of FPN, by exogenously added hepcidin, resulted in discrete changes not only in total cellular iron content but also in all three transverse relaxation rates (Figure 10). Exogenous hepcidin significantly influenced R_2 (Figure 10B), which reflected the same pattern of changes documented for R_2* (Figure 10A). These MR signals were influenced by both long-term (continuous iron supplementation) and short-term (within 24 hours of iron supplement withdrawal) changes in extracellular iron. By comparison, R_2' mainly displayed changes over shorter time scales, within 24 hours of removing iron supplement (Figure 10C). Moreover, in the presence of exogenous hepcidin, the correlations between total cellular iron content and transverse relaxation rates were all notable. R_2* displayed a significantly strong correlation to iron while both R_2 and R_2' showed moderate correlations. We note that both longitudinal and transverse relaxation rates identify a significant effect of hepcidin in the one-hour time frame (1h-Fe), possibly reflecting the short half-life of hepcidin and the transient nature of its activity. The changes in iron biochemistry that underlie these differential MR responses to autocrine/paracrine and endocrine hepcidin regulation of monocytes are considered below.

Monocyte iron biochemistry

Mammalian cells predominantly take up ferric iron (Fe^{+3}) through transferrin-TfRc interactions and store it as a biomineral in ferritin, in the ferrous state (Fe^{+2}). In humans, there is a positive correlation between serum ferritin and hepcidin indicating they work together to promote cellular iron storage [26]. The latter study also reported an increase in serum hepcidin expression during inflammation. It is not clear whether the stimulus, concentration and/or duration of the hepcidin signal influences the extent of monocyte responses to hepcidin activity. Our MR data suggest that iron-stimulated changes in FPN expression, resulting in autocrine/paracrine hepcidin activity, are distinct from endocrine hepcidin activity.

In our cell model, in the presence of extracellular iron supplementation (+Fe), there was no significant change in the cellular iron content compared to the untreated control (Figure 8A). Although another report suggested this may be due to an increase in FPN expression in iron-supplemented cells [27], we did not detect any change in iron export protein. While we have not ruled out the possibility that low TfRc expression limits iron uptake, following both hepcidin and extracellular iron treatment (+Fe, Figure 8B) we observed a significant increase in cellular iron content compared to unsupplemented controls (-Fe). This finding is consistent with a key role for iron export in the maintenance of monocyte iron homeostasis [28].

Another hypothesis is that hepcidin balances the fraction of iron stored in ferritin versus LIP, attenuating the net change in total cellular iron content. Since the form of iron cannot be determined through ICP-MS measurements, we have no indication of relative levels of iron in ferritin or LIP. This may be important to differentiate in the future as studies have shown increased ferritin mRNA expression due to hepcidin [19] as well as a positive correlation between monocyte LIP and hepcidin expression [29].

Where changes in MRI signal in the presence and absence of hepcidin are not corroborated by the quantification of iron, we speculate that differences in intracellular iron redox status may contribute to changes in transverse relaxivity. Dietrich *et al.* (2017) show a significant increase in R_2* of ferric (Fe^{+3}) compared to ferrous (Fe^{+2}) ions [30]. In

addition, House *et al.* (2007) emphasize that an increase in iron stored as ferritin may lead to an increase in R_2, partially consistent with our results [31]. The difference in correlation times (defined as the time required to rotate by approximately 1 radian) of dipolar interactions between the redox state(s) of iron and water protons contributes to changes in relaxation rates [30, 32, 33].

2.5 Conclusions

Differences in cellular iron handling mechanisms may allow some cell types to be tracked using MRI [34]. For example, monocytes are one of the most abundant immune cell types in chronic inflammatory conditions like atherosclerosis. In this context, hepcidin-mediated changes in iron retention may allow us to track the activity of these cells. Toward this goal, we examined human THP-1 monocytes and the effect of hepcidin on FPN protein expression, cellular iron content, and MR relaxation rates.

Since there was little or no change in FPN expression upon iron supplementation (+Fe), cellular iron content and MR relaxation rates remained unchanged compared to non-supplemented monocytes (-Fe). Following the withdrawal of iron supplement, cellular iron content remained constant; although, R_2* and R_2' significantly increased. In general, the addition of hepcidin lead to downregulation of FPN and a significant increase in cellular iron content. This finding was reflected in a significant increase in both longitudinal and transverse relaxation rates. Moreover, while iron content and R_2* were positively correlated in the absence of hepcidin, this moderate correlation was strengthened by the addition of hepcidin. These results demonstrate the effect of hepcidin on THP-1 monocyte iron regulation and the degree to which cellular iron content and regulation of iron export activity affect MRI measures. Overall, results from our *in vitro* study suggest that hepcidin-mediated changes in monocyte iron handling could potentially be tracked using MRI and may be exploited for monitoring inflammatory processes *in vivo*.

References

1. Fang L, Moore XL, Dart AM, Wang LM: **Systemic inflammatory response following acute myocardial infarction**. *J Geriatr Cardiol* 2015, **12**(3):305-312.
2. Wrigley BJ, Lip GYH, Shantsila E: **The role of monocytes and inflammation in the pathophysiology of heart failure**. *Eur J Heart Fail* 2011, **13**(11):1161-1171.
3. Rogacev KS, Cremers B, Zawada AM, Seiler S, Binder N, Ege P, Grosse-Dunker G, Heisel I, Hornof F, Jeken J: **CD14++CD16+ Monocytes Independently Predict Cardiovascular Events**. *J Am Coll Cardiol* 2012, **60**(16):1512-1520.
4. Deschemin JC, Vaulont S: **Role of Hepcidin in the Setting of Hypoferremia during Acute Inflammation**. *PLoS One* 2013, **8**(4):7.
5. Haschka D, Petzer V, Kocher F, Tschurtschenthaler C, Schaefer B, Seifert M, Sopper S, Sonnweber T, Feistritzer C, Arvedson TL: **Classical and intermediate monocytes scavenge non-transferrin-bound iron and damaged erythrocytes**. *JCI Insight* 2019, **4**(8):23.
6. Ben-Mordechai T, Holbova R, Landa-Rouben N, Harel-Adar T, Feinberg MS, Abd Elrahman I, Blum G, Epstein FH, Silman Z, Cohen S: **Macrophage subpopulations are essential for infarct repair with and without stem cell therapy**. *J Am Coll Cardiol* 2013, **62**(20):1890-1901.
7. Flogel U, Ding Z, Hardung H, Jander S, Reichmann G, Jacoby C, Schubert R, Schrader J: **In vivo monitoring of inflammation after cardiac and cerebral ischemia by fluorine magnetic resonance imaging**. *Circulation* 2008, **118**(2):140-148.
8. Le-Petross HT, Cristofanilli M, Carkaci S, Krishnamurthy S, Jackson EF, Harrell RK, Reed BJ, Yang WT: **MRI Features of Inflammatory Breast Cancer**. *Am J Roentgenol* 2011, **197**(4):W769-W776.
9. Payne AR, Berry C, Kellman P, Anderson R, Hsu L-Y, Chen MY, McPhaden AR, Watkins S, Schenke W, Wright V: **Bright-blood T2-weighted MRI has high diagnostic accuracy for myocardial hemorrhage in myocardial infarction: a preclinical validation study in swine**. *Circulation: Cardiovascular Imaging* 2011, **4**(6):738-745.

10. Smith PK, Krohn RI, Hermanson GT, Mallia AK, Gartner FH, Provenzano MD, Fujimoto EK, Goeke NM, Olson BJ, Klenk DC: **Measurement of protein using bicinchoninic acid**. *Anal Biochem* 1985, **150**(1):76-85.
11. Laemmli UK: **Cleavage of structural proteins during assembly of head of bacteriophage-T4**. *Nature* 1970, **227**(5259):680.
12. Towbin H, Staehelin T, Gordon J: **Electrophoretic transfer of proteins from polyacrylamide gels to nitrocellulose sheets - procedure and some applications**. *Proc Natl Acad Sci U S A* 1979, **76**(9):4350-4354.
13. Thomas C, Oates PS: **Ferroportin/IREG-1/MTP-1/SLC40A1 modulates the uptake of iron at the apical membrane of enterocytes**. *Gut* 2004, **53**(1):44-49.
14. Sengupta A, Quiaoit K, Thompson RT, Prato FS, Gelman N, Goldhawk DE: **Biophysical features of MagA expression in mammalian cells: implications for MRI contrast**. *Frontiers in Microbiology* 2014, **5**.
15. Ganz T: **Systemic iron homeostasis**. *Physiol Rev* 2013, **93**(4):1721-1741.
16. Kong WN, Lei YH, Chang YZ: **The regulation of iron metabolism in the mononuclear phagocyte system**. *Expert Rev Hematol* 2013, **6**(4):411-418.
17. Theurl I, Theurl M, Seifert M, Mair S, Nairz M, Rumpold H, Zoller H, Bellmann-Weiler R, Niederegger H, Talasz H *et al*: **Autocrine formation of hepcidin induces iron retention in human monocytes**. *Blood* 2008, **111**(4):2392-2399.
18. Cutone A, Frioni A, Berlutti F, Valenti P, Musci G, di Patti MCB: **Lactoferrin prevents LPS-induced decrease of the iron exporter ferroportin in human monocytes/macrophages**. *Biometals* 2014, **27**(5):807-813.
19. Jacolot S, Ferec C, Mura C: **Iron responses in hepatic, intestinal and macrophage/monocyte cell lines under different culture conditions**. *Blood Cells Mol Dis* 2008, **41**(1):100-108.
20. De Domenico I, Zhang TY, Koening CL, Branch RW, London N, Lo E, Daynes RA, Kushner JP, Li D, Ward DM: **Hepcidin mediates transcriptional changes that modulate acute cytokine-induced inflammatory responses in mice**. *J Clin Invest* 2010, **120**(7):2395-2405.

21. Nemeth E, Rivera S, Gabayan V, Keller C, Taudorf S, Pedersen BK, Ganz T: **IL-6 mediates hypoferremia of inflammation by inducing the synthesis of the iron regulatory hormone hepcidin**. *J Clin Invest* 2004, **113**(9):1271-1276.
22. Pagani A, Nai A, Corna G, Bosurgi L, Rovere-Querini P, Camaschella C, Silvestri L: **Low hepcidin accounts for the proinflammatory status associated with iron deficiency**. *Blood* 2011, **118**(3):736-746.
23. Park CH, Valore EV, Waring AJ, Ganz T: **Hepcidin, a urinary antimicrobial peptide synthesized in the liver**. *J Biol Chem* 2001, **276**(11):7806-7810.
24. Frangogiannis NG: **The inflammatory response in myocardial injury, repair, and remodelling**. *Nature Reviews Cardiology* 2014, **11**(5):255-265.
25. Ertl G, Frantz S: **Healing after myocardial infraction**. *Cardiovasc Res* 2005, **66**(1):22-32.
26. Ganz T, Olbina G, Girelli D, Nemeth E, Westerman M: **Immunoassay for human serum hepcidin**. *Blood* 2008, **112**(10):4292-4297.
27. Ludwiczek S, Aigner E, Theurl I, Weiss G: **Cytokine-mediated regulation of iron transport in human monocytic cells**. *Blood* 2003, **101**(10):4148-4154.
28. Andriopoulos B, Pantopoulos K: **Hepcidin generated by hepatoma cells inhibits iron export from co-cultured THP1 monocytes**. *Journal of Hepatology* 2006, **44**(6):1125-1131.
29. Risko P, Platenik J, Buchal R, Potockova J, Kraml PJ: **The labile iron pool in monocytes reflects the activity of the atherosclerotic process in men with chronic cardiovascular disease**. *Physiol Res* 2017, **66**(1):49-61.
30. Dietrich O, Levin J, Ahmadi SA, Plate A, Reiser MF, Botzel K, Giese A, Ertl-Wagner B: **MR imaging differentiation of Fe2+ and Fe3+ based on relaxation and magnetic susceptibility properties**. *Neuroradiology* 2017, **59**(4):403-409.
31. House MJ, St Pierre TG, Kowdley KV, Montine T, Connor J, Beard J, Berger J, Siddaiah N, Shankland E, Jin LW: **Correlation of proton transverse relaxation rates (R2) with iron concentrations in postmortem brain tissue from Alzheimer's disease patients**. *Magn Reson Med* 2007, **57**(1):172-180.

32. Gore JC, Kang YS, Schulz RJ: **Measurement of radiation-dose distributions by nuclear magnetic-resonance (NMR) imaging**. *Phys Med Biol* 1984, **29**(10):1189-1197.
33. Tokuhiro T, Appleby A, Leghrouz A, Metcalf R, Tokarz R: **Proton spin-lattice relaxation of water molecules in ferrous-ferric/agarose gel system**. *J Chem Phys* 1996, **105**(9):3761-3769.
34. Liu L, Alizadeh K, Donnelly SC, Dassanayake P, Hou TT, McGirr R, Thompson RT, Prato FS, Gelman N, Hoffman L *et al*: **MagA expression attenuates iron export activity in undifferentiated multipotent P19 cells**. *PLoS One* 2019, **14**(6):e0217842.

Chapter 3

3.1 Summary

In this study, iron regulation in THP-1 monocytes and its influence on MR relaxation rates were studied in the presence and absence of hepcidin. We found that (1) human THP-1 monocytes express FPN iron export protein in the presence and absence of extracellular iron and (2) FPN expression was downregulated in the presence of hepcidin. We showed that FPN downregulation is associated with an increase in cellular iron content, which likely promotes the observed increase in R_2* following hepcidin treatment of iron-supplemented cells. Furthermore, we showed that hepcidin-treated cells display a strong correlation between total cellular iron content and R_2*; whereas, in the absence of hepcidin, this was a moderate correlation. Overall, the results from this *in vitro* study may provide possibilities for *in vivo* tracking of hepcidin-mediated changes (*i.e.* due to inflammation) in monocyte iron-handling (*i.e.* due to hemorrhage) using MRI.

3.2 Future work

In this study, we examined the hepcidin-FPN interactions that govern mammalian iron regulation in THP-1 monocytes. In the presence of hepcidin, total cellular iron content is altered by changes in extracellular iron. Though these changes may reflect the downregulation of FPN by hepcidin, these findings should be further characterized in the future by investigating the expression levels of the iron import protein TfRc.

Although the total cellular iron content of monocytes increased in response to iron supplementation in the presence of hepcidin (Figure 4B), no changes in cellular iron content were observed between hepcidin treated cells and their untreated counterparts. However, differentiating these monocytes into macrophages and distinguishing between M1 (iron storage) and M2 (iron recycling) phenotypes may expose further differences in iron regulation [1]. Since these two phenotypes have distinct iron handling mechanisms, it would be interesting to investigate how changes in extracellular iron supplementation influence both the cellular iron content and MR relaxation rates [2, 3]. Since there may be a contribution from monocytes and macrophage phenotypes to the MR relaxation rates, it would be interesting to co-culture the monocytes and macrophages together and measure

the MR relaxation which would provide useful information to track inflammation *in vivo.* Also, it may be important to decipher whether any of these cells have the ability to produce hepcidin for autocrine and paracrine signalling [4], and that could be examined using basic lab techniques like the enzyme-linked immunosorbent assay (ELISA).

Changes in the iron redox state, from Fe^{+2} to Fe^{+3}, and how this influences MR relaxation rates are reported in the literature [5-7]. These changes in redox state may contribute to the significant increase in MR relaxation once the iron supplementation is withdrawn, regardless of hepcidin treatment, and may provide additional insight into monocyte iron regulation. In addition, a portion of total cellular iron in these monocytes exists as ferritin, representing iron bound to protein, or as iron within the transient LIP, representing unbound iron. Current literature indicates that ferritin-bound iron gives rise to R_2 relaxivity, while iron in the LIP gives rise to R_2* relaxivity [8, 9]. Therefore, quantifying the relative proportions of ferritin and LIP may provide insight into how iron form influences MR relaxation rates. Since iron metabolism is constantly readjusting to maintain homeostasis, we expect that the most sustained or long-lived changes would arise in the context of chronic inflammation or hemorrhage.

References

1. Recalcati S, Locati M, Marini A, Santambrogio P, Zaninotto F, De Pizzol M, Zammataro L, Girelli D, Cairo G: **Differential regulation of iron homeostasis during human macrophage polarized activation**. *Eur J Immunol* 2010, **40**(3):824-835.
2. Sabelli M, Montosi G, Garuti C, Caleffi A, Oliveto S, Biffo S, Pietrangelo A: **Human macrophage ferroportin biology and the basis for the ferroportin disease**. *Hepatology* 2017, **65**(5):1512-1525.
3. Jung M, Mertens C, Brune B: **Macrophage iron homeostasis and polarization in the context of cancer**. *Immunobiology* 2015, **220**(2):295-304.
4. Merle U, Fein E, Gehrke SG, Stremmel W, Kulaksiz H: **The iron regulatory peptide hepcidin is expressed in the heart and regulated by hypoxia and inflammation**. *Endocrinology* 2007, **148**(6):2663-2668.
5. Dietrich O, Levin J, Ahmadi SA, Plate A, Reiser MF, Botzel K, Giese A, Ertl-Wagner B: **MR imaging differentiation of Fe2+ and Fe3+ based on relaxation and magnetic susceptibility properties**. *Neuroradiology* 2017, **59**(4):403-409.
6. Gore JC, Kang YS, Schulz RJ: **Measurement of radiation-dose distributions by nuclear magnetic-resonance (NMR) imaging**. *Phys Med Biol* 1984, **29**(10):1189-1197.
7. Tokuhiro T, Appleby A, Leghrouz A, Metcalf R, Tokarz R: **Proton spin-lattice relaxation of water molecules in ferrous-ferric/agarose gel system**. *J Chem Phys* 1996, **105**(9):3761-3769.
8. Risko P, Platenik J, Buchal R, Potockova J, Kraml PJ: **The labile iron pool in monocytes reflects the activity of the atherosclerotic process in men with chronic cardiovascular disease**. *Physiol Res* 2017, **66**(1):49-61.
9. House MJ, St Pierre TG, Kowdley KV, Montine T, Connor J, Beard J, Berger J, Siddaiah N, Shankland E, Jin LW: **Correlation of proton transverse relaxation rates (R2) with iron concentrations in postmortem brain tissue from Alzheimer's disease patients**. *Magn Reson Med* 2007, **57**(1):172-180.

Appendix A: Raw data of relaxation rates for THP-1 monocytes in response to changes in extracellular iron supplementation.

R_1 Relaxation rate					Mean	SD	SEM
-Fe	0.83	0.79	0.89		0.84	0.05	0.03
+Fe	0.85	0.84	0.84		0.84	0.01	0.003
1h-Fe	0.96	1.09	0.85		0.96	0.12	0.06
2h-Fe	1.05	1.09	0.84		0.99	0.13	0.07
4h-Fe	0.95	0.99	0.92		0.95	0.03	0.02
24h-Fe	0.72	0.84	0.80		0.78	0.06	0.03

R_2* Relaxation rate					Mean	SD	SEM
-Fe	16.86	12.51	14.49	13.00	14.22	1.95	0.98
+Fe	10.01	15.75	16.56	15.84	14.54	3.04	1.52
1h-Fe	20.98	21.06	28.13	22.65	23.21	3.37	1.69
2h-Fe	23.66	27.62	28.98	21.94	25.55	3.30	1.65
4h-Fe	24.38	26.00	22.17		24.18	1.92	1.11
24h-Fe	14.06	14.21	14.77		14.35	0.37	0.22

R_2 Relaxation rate					Mean	SD	SEM
-Fe	12.5	10.66	10.14	11.37	11.17	1.02	0.51
+Fe	5.45	11.98	11.80	11.85	10.27	3.21	1.61
1h-Fe	13.70	12.72	16.39	13.47	14.07	1.60	0.80
2h-Fe	13.34	13.95	16.15	13.4	14.21	1.32	0.66
4h-Fe	17.04	17.44	13.59		16.02	2.12	1.22
24h-Fe	8.37	10.44	9.86		9.56	1.07	0.62

R_2' Relaxation rate					Mean	SD	SEM
-Fe	4.36	1.85	4.35	1.63	3.05	1.51	0.76
+Fe	4.56	3.77	4.76	3.99	4.27	0.47	0.23
1h-Fe	7.28	8.34	11.74	9.18	9.14	1.90	0.95
2h-Fe	10.32	13.67	12.83	8.54	11.34	2.35	1.17
4h-Fe	7.34	8.56	8.58		8.16	0.71	0.41
24h-Fe	5.69	3.77	4.91		4.79	0.97	0.56

Appendix B: Raw data of relaxation rates for THP-1 monocytes in response to changes in extracellular iron supplementation and hepcidin

R_1 Relaxation rate					Mean	SD	SEM
-Fe	0.72	0.72	0.75		0.73	0.02	0.01
+Fe	0.94	0.84	0.86		0.88	0.05	0.03
1h-Fe	0.79	0.82	0.83		0.81	0.02	0.01
2h-Fe	0.89	0.90	0.90		0.89	0.01	0.003
4h-Fe	0.96	0.97	0.96		0.96	0.01	0.003
24h-Fe	0.80	0.81	0.82		0.81	0.01	0.01

R_2* Relaxation rate					Mean	SD	SEM
-Fe	12.94	12.45	14.21		13.20	0.91	0.52
+Fe	20.75	19.29	21.13		20.39	0.97	0.56
1h-Fe	15.70	16.27	16.88	17.75	16.65	0.88	0.44
2h-Fe	29.05	23.88	29.36		27.43	3.10	1.78
4h-Fe	26.05	21.52	26.08		24.55	2.62	1.52
24h-Fe	14.72	11.89	17.67		14.76	2.89	1.67

R_2 Relaxation rate					Mean	SD	SEM
-Fe	7.73	8.30	8.63		8.22	0.46	0.26
+Fe	13.30	12.37	11.37		12.35	0.97	0.56
1h-Fe	9.83	11.06	11.02	11.93	10.96	0.86	0.43
2h-Fe	15.32	13.78	17.56		15.55	1.90	1.10
4h-Fe	16.00	14.48	20.16		16.88	2.94	1.70
24h-Fe	9.76	9.90	10.59		10.08	0.44	0.26

R_2' Relaxation rate					Mean	SD	SEM
-Fe	5.21	4.15	5.58		4.98	0.74	0.43
+Fe	7.45	6.92	10.11		8.16	1.71	0.99
1h-Fe	5.87	5.21	5.86	5.82	5.69	0.32	0.16
2h-Fe	13.73	10.10	12.30		12.04	1.83	1.06
4h-Fe	10.50	10.94	5.92		9.12	2.78	1.61
24h-Fe	4.96	1.94	6.54		4.48	2.34	1.35

Appendix C: Raw data of densitometry indicating the ratio between FPN and GAPDH: without hepcidin

Densitometry (FPN/GAPDH)						
Experiment	1	2	3	Mean	SD	SEM
-Fe	1.050	0.994	0.951	0.998	0.05	0.03
+Fe	1.120	1.060	0.930	1.037	0.10	0.06
1h-Fe	0.458	0.016	0.500	0.324	0.20	0.15
2h-Fe	0.387	0.500	0.383	0.423	0.07	0.04
4h-Fe	1.150	0.900	0.757	0.936	0.20	0.12
24h-Fe	0.290	0.029	0.050	0.123	0.15	0.08

Appendix D: Raw data of densitometry indicating the ratio between FPN and GAPDH: with hepcidin

Densitometry (FPN/GAPDH)						
Experiment	1	2	3	Mean	SD	SEM
-Fe	0.409	0.453	0.423	0.428	0.02	0.01
+Fe	0.564	0.583	0.507	0.551	0.04	0.02
1h-Fe	0.493	0.363	0.715	0.552	0.18	0.10
2h-Fe	0.246	0.256	0.352	0.285	0.06	0.03
4h-Fe	0.211	0.163	0.292	0.222	0.07	0.04
24h-Fe	0.141	0.145	0.168	0.151	0.02	0.01

Appendix E: Western blots

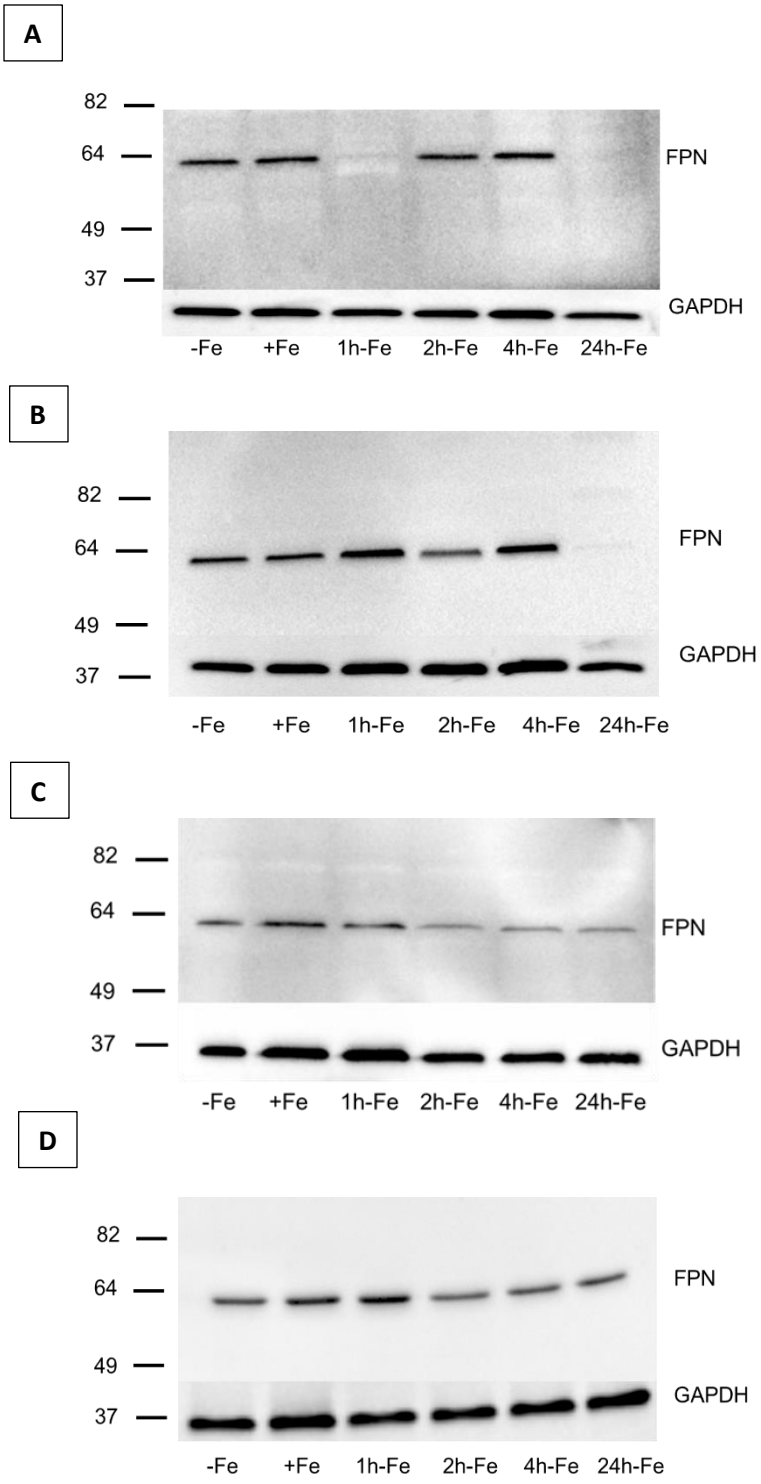

Figure 1. Regulation of ferroportin (FPN) expression in THP-1 monocytes by extracellular iron and hepcidin. THP-1 cells were cultured for 7 days in the absence (-Fe) or presence (+Fe) of iron-supplemented medium containing 25μM ferric nitrate. Cells were either harvested immediately or after the withdrawal of iron supplement and culture for an additional 1 (1h-Fe), 2 (2h-Fe), 4 (4h-Fe) and 24 (24h-Fe) hours. To examine FPN regulation, -Fe and +Fe samples were grown in the presence of 200 ng/ml hepcidin for the last 24 hours of culture while hepcidin was added to all other samples after the removal of iron supplement. Representative Western blots show the change in FPN expression in the absence (A and B) and presence (C and D) of hepcidin. Molecular weight standards are indicated on the left while GAPDH provided a loading control.

Appendix F: Exponential curves

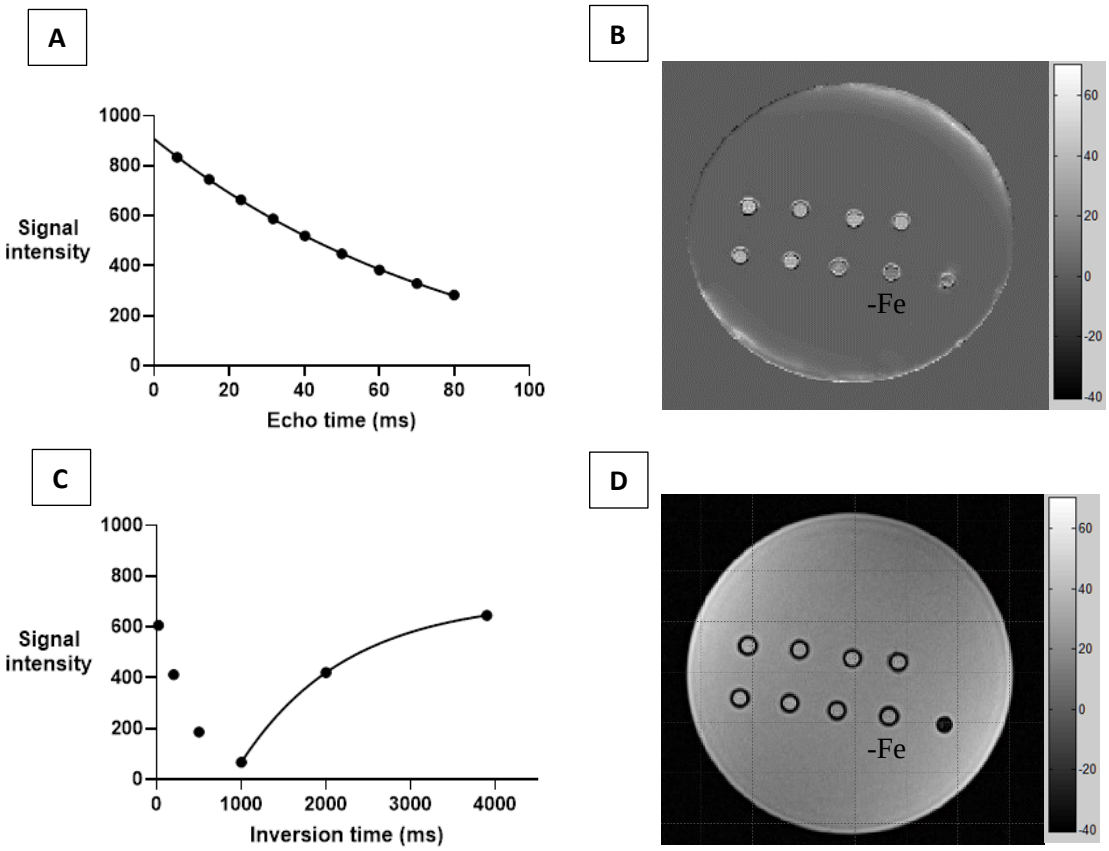

Figure 2. Exponential curves of transverse and longitudinal relaxation rates. A. Signal decay curve is shown for T_2* weighted images for -Fe control condition. Each point on the graph represents mean signal intensity measured within a defined ROI and plotted against echo times. Exponential fitting was conducted to calculate the transverse relaxation rate (R_2*). **B**. The R_2* map, representing the phantom was obtained using voxel by voxel exponential curve fitting **C.** Signal growth curve is shown for T_1 weighted images for the -Fe control condition. Each point on the graph represents mean signal intensity measured within a defined ROI and plotted against echo times. Exponential fitting was conducted to calculate the longitudinal relaxation rate (R_1). **D.** The R_1 map representing the phantom was obtained using voxel by voxel exponential curve fitting.

Curriculum Vitae

Name: Praveen Dassanayake

Post-secondary Education and Degrees:

M.Sc Candidate, Medical Biophysics
Western University, London, ON
2017-Present

B.Sc, Physics
University of Sri Jayewardenepura, Sri Lanka
2013-2016

Honours and Awards:

Travel Award, Institute Community Support
Canadian Institutes of Health Research (CIHR), Canada
November 2018

Travel Award, Molecular Imaging Program
University of western Ontario
September 2018

Related work Experience:

Teaching Assistant
Department of Physics
University of Sri Jayewardenepura, Sri Lanka
2016-2017

Publications

Manuscripts

- Liu, L., Alizadeh, K., Donnelly, S.C., Dassanayake, P., Hou, T.T., McGirr, R., Thompson, R.T., Prato, F.S., Gelman, N., Hoffman, L. and Goldhawk, D.E., 2019. MagA expression attenuates iron export activity in undifferentiated multipotent P19 cells. PloS one, 14(6).

Abstracts

- P. Dassanayake, O.C Sehl, N. Gelman, R.T. Thompson, F.S. Prato, D.E. Goldhawk. Investigating the correlation between cellular iron content and magnetic resonance signal using THP-1 monocytes to model the inflammatory response, Imaging network of Ontario (ImNO), Toronto, Ontario, Canada, March 2018.

- P. Dassanayake, O.C Sehl, N. Gelman, R.T. Thompson, F.S. Prato, D.E. Goldhawk., Monitoring Inflammation Using THP-1 Monocytes and Magnetic Resonance Imaging, London Health Research Day, London, Ontario, Canada, May 2018.

- P. Dassanayake, O.C Sehl, N. Gelman, R.T. Thompson, F.S. Prato, D.E. Goldhawk. Differentiating pro- and anti-inflammatory response using THP-1 monocytes and magnetic resonance imaging, World Molecular Imaging Congress, Seattle, USA, September 2018.

- P. Dassanayake, N. Gelman, R.T. Thompson, F.S. Prato, D.E. Goldhawk. Examining the effect of hepcidin on cardiac inflammation using THP-1 monocytes and MRI, Imaging network of Ontario (ImNO), London, Ontario, Canada, March 2019

- P. Dassanayake, N. Gelman, R.T. Thompson, F.S. Prato, D.E. Goldhawk. THP-1 Monocyte MRI Relaxation Rates are Regulated by Extracellular Iron and Hepcidin, London Health Research Day, London, Ontario, Canada, April 2019